

# A long-term dataset of simulated epilimnion and hypolimnion temperatures in 401 French lakes (1959-2020)

Najwa Sharaf<sup>1,2</sup>, Jordi Prats<sup>3</sup>, Nathalie Reynaud<sup>1,2</sup>, Thierry Tormos<sup>1,4</sup>, Rosalie Bruel<sup>1,4</sup>,  
Tiphaine Peroux<sup>1,2</sup>, Pierre-Alain Danis<sup>1,4</sup>

<sup>1</sup>Pôle R&D Ecosystèmes Lacustres (ECLA), OFB-INRAE-USMB, Aix-en-Provence, France

<sup>2</sup>INRAE, Aix Marseille Univ, RECOVER, Team FRESHCO, 3275 Route Cézanne, 13182 Aix-en-Provence, France

<sup>3</sup>SEGULA Technologies, C. Calàbria 169, 08015 Barcelona, Spain

<sup>4</sup>OFB, DRAS, Service ECOAQUA, 3275 Route Cézanne, 13100 Aix-en-Provence, France

*Correspondence to:* Sharaf Najwa ([najwa.sharaf@inrae.fr](mailto:najwa.sharaf@inrae.fr)), Bruel Rosalie ([rosalie.brue@ofb.gouv.fr](mailto:rosalie.brue@ofb.gouv.fr)), Tormos Thierry ([thierry.tormos@ofb.gouv.fr](mailto:thierry.tormos@ofb.gouv.fr)), Reynaud Nathalie ([nathalie.reynaud@inrae.fr](mailto:nathalie.reynaud@inrae.fr))

54 **1. Abstract**

55 Understanding the thermal behavior of lakes is crucial for water quality management. Under climate change, lakes  
56 are warming and undergoing alterations in their thermal structure, including surface and deep-water temperatures.  
57 These changes require continuous monitoring due to the possible major ecological implications on water quality  
58 and lake processes. We combined numerical modelling and satellite thermal data to create a regional dataset  
59 (LakeTSim: Lake Temperature Simulations) of long-term water temperatures for 401 French lakes in order to  
60 tackle the scarcity of in situ water temperature (Sharaf et al., 2023; [doi:10.57745/OF9WXR](https://doi.org/10.57745/OF9WXR)). The dataset consists  
61 of daily epilimnion and hypolimnion water temperatures for the period 1959-2020 simulated with the semi-  
62 empirical OKPLM (Ottosson-Kettle-Prats Lake Model) and the associated uncertainties. Here, we describe the  
63 model and its performance. Additionally, we present the uncertainty analysis of simulations with default parameter  
64 values (parametrized as a function of lake characteristics) and calibrated parameter values, along with the analysis  
65 of the sensitivity of the model to parameter values and biases in the input data. Overall, the 90% confidence  
66 uncertainty range is largest for hypolimnion temperature simulations with a median of 8.5 °C and 2.32 °C  
67 respectively with default and calibrated parameter values. There is less uncertainty associated with epilimnion  
68 temperature simulations with a median of 5.42 °C and 1.85 °C, respectively before and after parameter calibration.  
69 This dataset provides over six decades of epilimnion and hypolimnion temperature data, crucial for climate change  
70 studies at a regional scale. It will help provide insight into the thermal functioning of French lakes and can be used  
71 to help decision-making and stakeholders.

72 **2. Introduction**

73 Lakes, both natural and artificial (i.e., reservoirs and gravel pits) are sentinels of environmental change and provide  
74 important services such as access to drinking water, hydropower production, recreation and fisheries (Adrian et  
75 al., 2009). Under climate change and anthropogenic pressures, many lakes are warming and consequently  
76 experiencing changes to their biophysicochemical structure and function that are leading to services being  
77 compromised (Janssen et al., 2021).

78 In lakes, water temperature is an essential parameter regulating processes such as the functioning of trophic webs,  
79 oxygen conditions, the physical structure of the water column as well as the biogeochemistry (Yang et al., 2018).  
80 Under warming, historical records and future projections demonstrate that for lakes, alterations in the  
81 thermodynamic functioning including warmer temperatures and shifts in mixing regimes already took place and  
82 are expected to persist in the future (Shatwell et al., 2019; Woolway and Merchant, 2019). In this context, they are  
83 undergoing shorter periods of ice cover and longer, more stable periods of thermal stratification (Woolway et al.,  
84 2022). These alterations could have considerable ecological implications for the biological communities (Lind et  
85 al., 2022; Havens and Jeppesen, 2018). For instance, worldwide studies have shown that the expansion of toxic  
86 cyanobacterial blooms is linked to warming (Griffith and Gobler, 2020). Other responses include species reduced  
87 body size (Daufresne et al., 2009), changes in thermal habitat and shifts in species seasonality (Kharouba et al.,  
88 2018).

89 It is thus crucial to closely evaluate water temperature trajectories over the entire water column in space and time  
90 when assessing the impact of climate change on lake ecosystems. However, the lack of data coverage, both  
91 spatially and temporally, makes it difficult to accurately characterize lakes thermal response to climate change and  
92 to identify warming trends (Gray et al., 2018). Indeed, long-term datasets of in situ temperatures are usually scarce

93 and mostly limited to large lakes (Layden et al., 2015). Moreover, sampling frequency and temporal coverage of  
94 in situ water temperature varies greatly from one lake to the next, from a few years (Sharma et al., 2015) up to  
95 decades (Piccolroaz et al., 2020; Rimet et al., 2020).

96 Due to the difficulties in setting up conventional (i.e., in situ) monitoring programs tied to e.g., costs, governance  
97 and intercalibration, the coupling of modelling and satellite remote sensing data has become fundamental in the  
98 field of limnology (Nouchi et al., 2019). Modelling provides means to interpolate both temporal and spatial gaps.  
99 It thereby allows us to acquire information about surface water temperatures, which are globally the focus of lake  
100 climate change studies, and deep-water temperatures which are as critical though often disregarded in this context  
101 (however see Pilla et al., 2020). Several numerical models that vary in complexity exist for conducting water  
102 temperature simulations, the most accurate being deterministic or process-based models. Nevertheless, regional or  
103 global deterministic modelling efforts over long periods are usually hindered by the lack of sufficiently detailed  
104 input data (e.g., meteorological and field data) to run the models (Kim et al., 2021). For practical and operational  
105 purposes, simpler models (semi-empirical, statistical or hybrid physical-statistical based models) with less  
106 requirements for forcing data, have been mostly applied to assess the impact of climate change on lake ecosystems  
107 and study them (Piccolroaz et al., 2020; Toffolon et al., 2014; Sharma et al., 2008). Long-term simulations across  
108 a considerable number of lakes are made possible with this type of models, enabling the detection of trends in time  
109 series data that are not achievable with shorter datasets (Gray et al., 2018).

110 The performance of numerical models depends highly on the calibration of their parameters as well as on the  
111 quality of the input data. Satellite remote sensing is an effective way to monitor surface water temperature on a  
112 synoptic scale (Schaeffer et al., 2018; Sharaf et al., 2019) and provide a complementary source of data to in situ  
113 measurements for model calibration or validation purposes (Allan et al., 2016; Babbar-Sebens et al., 2013). In  
114 particular, thermal infrared sensors onboard the Landsat satellites are very adequate for retrospective analysis of  
115 surface water temperature with a spatial resolution adapted for small to medium size lakes and reservoirs at a  
116 bimonthly acquisition frequency. Landsat 4 and 5 TM (Thematic Mapper), 7 ETM+ (Enhanced Thematic Mapper)  
117 and 8 TIRS (Thermal InfraRed Sensor) provide surface temperature data at spatial resolutions of 120, 60 and 100  
118 m respectively. Landsat series records of surface water temperature can be used to validate 3D hydrodynamic  
119 models when in situ measurements are scarce (Sharaf et al., 2021) and to spatially assess the quality and suitability  
120 of aquatic habitat for biological communities (Halverson et al., 2022). Although, satellite thermal data is limited  
121 to the surface, its integration into model calibration could improve the accuracy of simulations over the surface  
122 layer and the water column (Javaheri et al., 2016).

123 Here we present on a regional scale, a long-term dataset, LakeTSim (Lake Temperature Simulations), of daily  
124 epilimnion and hypolimnion temperature simulations, as well as uncertainties, for the period 1959-2020 over 401  
125 French lakes monitored under the Water Framework Directive (WFD) including natural and artificial lakes,  
126 reservoirs and gravel pits. We present the OKPLM (Ottosson-Kettle-Prats Lake Model) used to produce water  
127 temperature simulations and its performance. Further, we provide the uncertainty analysis of simulations with  
128 default (parametrized with in situ and satellite thermal data over an entire set of lakes) and calibrated (with in situ  
129 temperature measurements for each lake) model parameter values as well as the sensitivity analysis for the latter.  
130 The goal of publishing this dataset is to provide new insight about epi- and hypolimnion temperatures of lakes in  
131 France especially for those that are not monitored regularly through conventional methods. This long-term dataset

132 is valuable for developing temperature indicators for identifying warming trends, extreme events and possible  
133 changes in the mixing regime among others. These indicators will contribute to assess the impact of climate change  
134 on lakes thermal functioning and its influence on the biological community structure and trophic webs.

### 135 **3. Data and methodology**

#### 136 **3.1. The software suite ALAMODE**

137 The simulations, sensitivity and uncertainty analysis presented in this paper were made using the software suite  
138 ALAMODE (A LAke MODElling project). ALAMODE (Danis, 2020) is a software suite developed in python 3  
139 by the Pôle R&D Ecosystèmes Lacustres (ECLA) and SEGULA Technologies to facilitate the realization of  
140 simulations of lakes and the management of related information. It comprises multiple modules and packages  
141 designed for lake and tributary modelling, as well as for processing the data necessary to operate these models.  
142 These packages include OKPLM (Ottosson-Kettle-Prats Lake Model), CUSPY (Calibration, Uncertainty analysis  
143 and Sensitivity analysis in PYthon), TMOD (Temperature MODElling), GLMtools (General Lake Model tools),  
144 “tributary”, TINDIC (Temperature INDICators) and ALAPROD (ALAMODE-Production). OKPLM (Prats-  
145 Rodríguez and Danis, 2023b) is used to simulate epilimnion and hypolimnion water temperatures in lakes while  
146 CUSPY (Prats-Rodríguez and Danis, 2023a) is used for model parameters estimations and conducting uncertainty  
147 and sensitivity analyses. TMOD is used for managing the T-MOD database designated to facilitate the realization  
148 and consultation of simulations. GLMtools is used to conduct lake hydrodynamic simulations using the one-  
149 dimensional hydrodynamic General Lake Model (Hipsey et al., 2019) while “tributary” is used for the estimation  
150 of flow and temperature of lake tributaries. The package TINDIC is used for calculating temperature indicators  
151 from model simulations. Finally, ALAPROD integrates all the functionalities to produce simulations into a single  
152 package: simulation of stream water temperature, of lake hydrodynamics and temperature, and of stream flow rate.  
153 It also includes sensitivity and uncertainty analysis features. The functionalities of these packages can be accessed  
154 either by using each package separately or by utilizing the ALAPROD package, which depends on the TMOD  
155 database and requires access to it.

156 At present, only the ALAMODE packages related to the main functionalities used in this work are publicly  
157 available (see Code availability section): the simulation of lake temperatures using the Ottosson-Kettle-Prats Lake  
158 Model (Prats & Danis, 2019), implemented in the package OKPLM, and the sensitivity and uncertainty analysis  
159 tools in the CUSPY package. We used ALAPROD to access the functionalities of both packages.

#### 160 **3.2. The OKP Lake Model description**

161 The OKPLM (Ottosson-Kettle-Prats Lake Model) (Prats & Danis, 2019) is a two-layer semi-empirical data model  
162 adapted from Kettle et al (2004) for the epilimnion module and Ottosson & Abrahamsson (1998) for the  
163 hypolimnion module. The modifications proposed in Prats & Danis (2019) consisted mainly of simplifying the  
164 mixing algorithm used in Ottosson & Abrahamsson (1998) using a basic stability condition, whereas for the  
165 epilimnion module a sinusoidal fit to average daily solar radiation was used instead of the theoretical clear-sky  
166 radiation. The OKPLM also runs on weekly and monthly frequencies. The regionalization of the parameters of the  
167 model mainly depends on the geographical and morphological properties of the lake (maximal depth, volume,  
168 surface area, latitude and altitude). The model requires few meteorological forcing data: solar radiation and air  
169 temperature.

170 The model calculates water temperature as follows:

$$171 \quad T_{e,i} = A + Bf(T_{a,i}^*) + CS_i \quad (1)$$

172 where  $T_e$  is the epilimnion temperature (°C),  $i$  is the day number,  $A$ ,  $B$  and  $C$  are calibration parameters,  $S$  is the  
173 solar radiation ( $\text{W m}^{-2}$ ) and  $f(*)$  is an exponential smoothing function with  $T_{a,i}^*$  defined as:

$$174 \quad T_{a,i}^* = T_{a,i} - MAAT \quad (2)$$

175 Where  $T_{a,i}$  is air temperature (°C) and  $MAAT$  is the annual mean air temperature (°C). The smoothing function  
176  $f(*)$  is such that it gives greater weight to the nearest observations and the weights decrease exponentially. It is  
177 defined as:

$$178 \quad f(T_{a,1}^*) = T_{a,1}^* \quad (3)$$

$$179 \quad f(T_{a,i}^*) = \alpha T_{a,i}^* + (1 - \alpha)f(T_{a,i-1}^*) \quad (4)$$

180 where  $\alpha$  is the smoothing factor. When  $\alpha = 1$  there is no smoothing, while the smoothing increases with the  
181 decrease in the value of  $\alpha$ .

$$182 \quad T_{h,i} = A \cdot D + E \cdot g(T_{e,i}) \quad (5)$$

183 where  $T_h$  is the hypolimnion temperature (°C),  $D$  and  $E$  are calibration parameters and  $g(T_{e,i})$  is an exponential  
184 smoothing as follows:

$$185 \quad g(T_{e,1}) = T_{e,1} \quad (6)$$

$$186 \quad g(T_{e,i}) = \beta T_{e,i} + (1 - \beta)g(T_{e,i-1}) \quad (7)$$

187 where  $\beta$  is the exponential smoothing factor. As for  $\alpha$ , there is no smoothing for  $\beta = 1$  and the smoothing increases  
188 as  $\beta$  approaches zero.

189 In ALAPROD, OKPLM can be run in two modes: the “default” mode where model parameter values for each  
190 lake are estimated using the parameterization presented in Prats & Danis (2019), and the “calibrated” mode where  
191 model parameters are calibrated individually for each lake by using in situ temperature measurements. The default  
192 parameterization was obtained by using the individually calibrated parameter values to fit appropriate expressions  
193 as a function of the characteristics of lakes. In the epilimnion module model parameter values  $A$ ,  $B$ ,  $C$ , and  $\alpha$  are  
194 estimated based on lake characteristics (i.e., latitude, altitude, surface area, volume, and depth). These equations  
195 were determined using robust regressions and Landsat infrared data (median skin temperatures) from 1999 to 2016  
196 of French lakes to estimate mean surface temperatures (Prats et al., 2018). In contrast, for the hypolimnion module,  
197 parameter values  $E$  and  $\beta$  were derived as a function of lake depth and lake type using temperature profile data  
198 from 357 lakes;  $\beta$  can have a value of 1 ( $E > 0.95$ ) or 0.13 ( $E \leq 0.95$ ). The parameter  $D$  was assigned a constant  
199 value of 0.51.

200 The parametrization of the OKPLM parameters as presented in Prats & Danis (2019) is as follows:

$$201 \quad A = 39.9 - 0.484L_{Lat} - 4.52 \times 10^{-3}L_{Alt} - 0.167\ln L_A \quad (8)$$

202 where  $L_{Lat}$  is lake latitude ( $^{\circ}$ N),  $L_{Alt}$  is lake altitude (m) and  $L_A$  is lake surface area ( $m^2$ ).

$$203 \quad B = 1.058 - 0.0010L_{Dmax} \quad (9)$$

204 where  $L_{Dmax}$  is lake maximal depth (m).

$$205 \quad C = 1.12 \times 10^{-3} - 3.62 \times 10^{-6}L_{Alt} \quad (10)$$

$$206 \quad E = e_1 + \frac{1-e_1}{1+\exp[e_3(e_2-\ln L_D)]} \quad (11)$$

207 where  $e_1$ ,  $e_2$  and  $e_3$  are coefficients with respective values of 0.10, 2.0, -1.8 for natural lakes and 0.49, 1.7, -2.0  
208 for artificial lakes (reservoirs, gravel pits, ponds and quarry lakes) and  $L_D$  is lake mean depth (m).

$$209 \quad \alpha = \exp(0.52 - 3.0 \times 10^{-4}L_{Alt} + 0.25\ln L_A - 0.36\ln L_V) \quad (12)$$

210 where  $L_V$  is lake volume ( $m^3$ ).

### 211 **3.3. Input data**

212 The OKPLM was forced with two sources of meteorological data extracted from the SAFRAN (Système d'Analyse  
213 Fournissant des Renseignements Adaptés à la Nivologie) analysis system (Durand et al., 1993) and the S2M  
214 (SAFRAN–SURFEX/ISBA–Crocus–MEPRA) meteorological reanalysis (Vernay et al., 2015, 2022).

215 The SAFRAN system provides meteorological variables at an hourly time step estimated through interpolation  
216 and assimilation processes with an 8 km square grid. Average daily data from the nearest grid cell was selected  
217 for each study site. The difference in altitude between the study site and the grid cell was accounted for by applying  
218 an adiabatic elevation correction on air temperature.

219 The S2M model chain combines the SAFRAN meteorological analysis and the SURFEX/ISBA–Crocus snow  
220 cover model including MEPRA (Modèle Expert d'Aide à la Prévision du Risque d'Avalanche). It is more adapted  
221 to mountainous regions as it has a spatial definition where spatial heterogeneity is taken into consideration. The  
222 S2M reanalysis uses a vertical resolution of 300 m and is the result of simulations performed over mountainous  
223 zones referred to as “massifs” and covering the French Alps, Pyrenees and Corsica mountainous regions. In order  
224 to use S2M meteorological data over each lake an extraction of certain topographic classes is necessary. These  
225 include elevation, aspect and slope, which represent the spatial variability over “massifs”. On average, a massif  
226 corresponds to a mountainous region of about 1000  $km^2$  over which meteorological conditions are considered  
227 homogeneous at a given elevation range. Two types of S2M reanalysis simulations exist for each elevation range,  
228 one at flat terrain and the other with 8 aspects at 2 different slope angles. For this study, this information (elevation,  
229 slope, aspect) was extracted from a Digital Elevation Model (BD Alti, IGN) for each lake over its drainage basin,  
230 combined into zones corresponding to S2M topographic classes. We considered a zero slope and average daily  
231 data for each study site.

232 In situ temperature profiles, geographical and morphological data of the study sites were initially extracted from  
233 the PLAN\_DEAU database. The extracted data was then incorporated into the T-MOD database, with the aim of  
234 simplifying the process of simulations and accessing information about the characteristics of the simulated lakes.  
235 Both databases are managed by INRAE (l'Institut National de Recherche pour l'Agriculture, l'Alimentation et  
236 l'Environnement) and Pôle R&D ECLA ("ECosystèmes Lacustres") in Aix-en-Provence, France. The

237 geomorphological data consisting of maximal depth, volume, surface area, latitude and altitude were extracted for  
238 401 lakes. In situ temperature profiles were extracted from the RCS/RCO (Réseau de Contrôle de  
239 Surveillance/Réseau de Contrôle Opérationnel, French networks for the Water Framework Directive (WFD))  
240 monitoring network for 170 lakes over different depths. Depending on each lake, the number of years with samples  
241 could vary from 1 to 12 with a number of samples ranging between 1 and 10 per year.

#### 242 **3.4. Lake simulations**

243 For this study, we considered 401 lakes (Figure 1) located in Metropolitan France monitored according to the  
244 WFD. Here we refer to lakes as natural lakes, reservoirs, gravel pits and other artificial lakes (e.g., ponds and  
245 quarry lakes). The present lake dataset includes epi- and hypolimnion temperature simulations for 54 natural lakes,  
246 302 reservoirs, 7 gravel pits and 38 other artificial lakes (Figure 2). The lakes characteristics range between 0 and  
247 2279.7 m for altitude, 0.8 and 309.7 m for maximal depth, 0.08 and 577.12 km<sup>2</sup> for surface area and  $5 \times 10^4$  and  
248  $8.9 \times 10^{10}$  m<sup>3</sup> for volume.

249 The OKPLM was run for each lake using either “default” or “calibrated” parameters, and either SAFRAN or S2M  
250 meteorological data. Specifically, “calibrated” model parameters were adopted when in situ temperature profiles  
251 along the water columns were available from the RCS/RCO monitoring network; these temperature profiles were  
252 then transformed and used as epilimnion and hypolimnion temperatures. For those lakes, calibration parameters  
253 ( $A$ ,  $B$ ,  $C$ ,  $D$ ,  $E$ ,  $\alpha$  and  $\beta$ ) are lake-specific and determined using the lake-specific temperature profiles. Conversely,  
254 “default” parameters were used for the rest of the lakes as well as when bathymetry data necessary for the  
255 transformation of temperature profiles into epilimnion and hypolimnion temperatures were not available. In this  
256 case, the values of the parameters were estimated according to equations (8) to (12).

257 SAFRAN data were used for most of the lakes except for a few lakes at higher altitudes. Indeed, S2M data are  
258 more representative of mountainous meteorological conditions than SAFRAN data and were thus used, when  
259 possible, for simulating the water temperature in lakes situated at altitudes higher than 900 m. For some lakes, it  
260 was not possible to use S2M data, either because their drainage basins are not entirely part of a massif ( $n = 1$ ), or  
261 because they are located in massifs that are not covered by the S2M reanalysis dataset ( $n = 18$ ). Among the total  
262 number of study sites ( $n = 401$ ), the model was forced using SAFRAN and S2M meteorological data respectively  
263 for 210 and 21 lakes with “default” model parameters, and for 164 and 6 lakes with “calibrated” model parameters.  
264 The geomorphological characteristics of the simulated lakes with each of the abovementioned configurations are  
265 shown in Table 1.

266

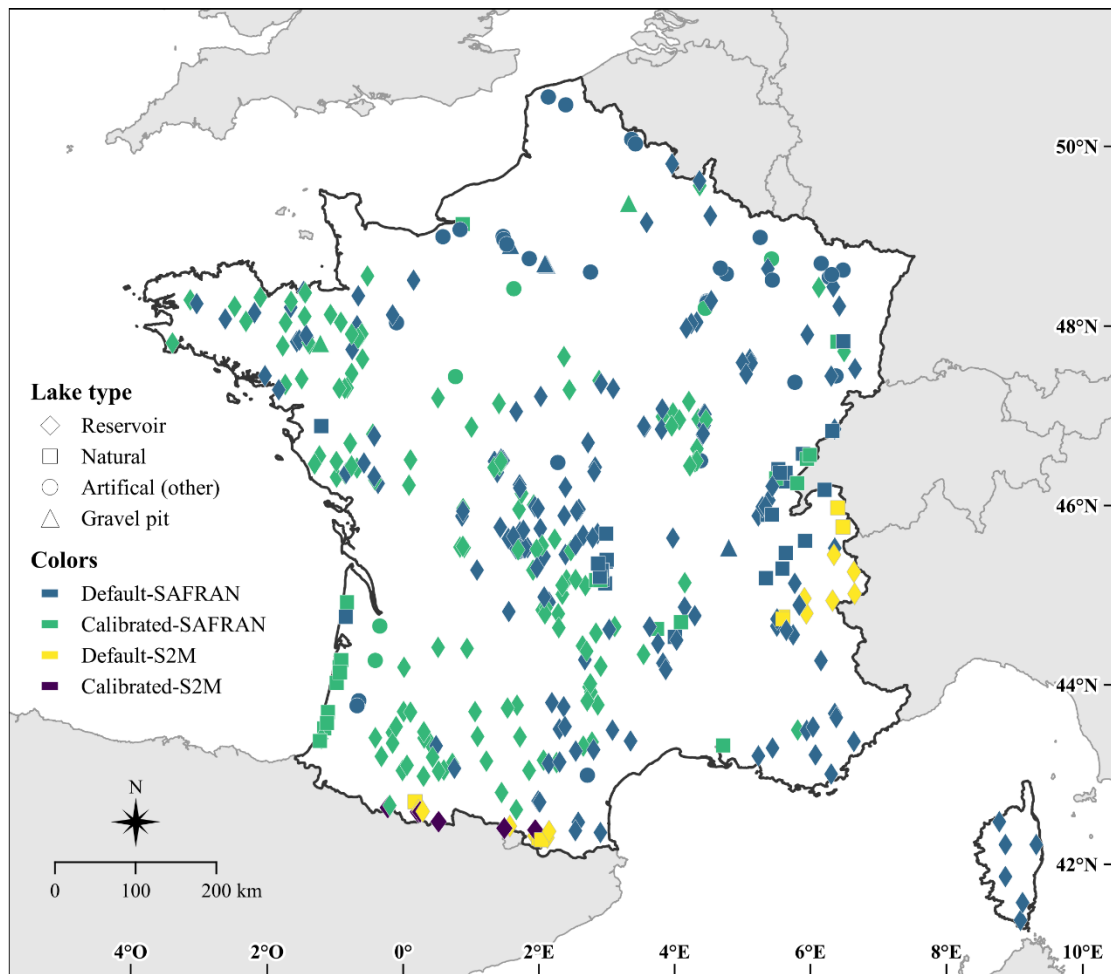


**Figure 1: Location and lake type of the 401 French lakes simulated with the OKPLM in “default” and “calibrated” modes, with SAFRAN and S2M meteorological data for the period 1959-2020. The “other” artificial lakes consist of ponds and quarry lakes.**



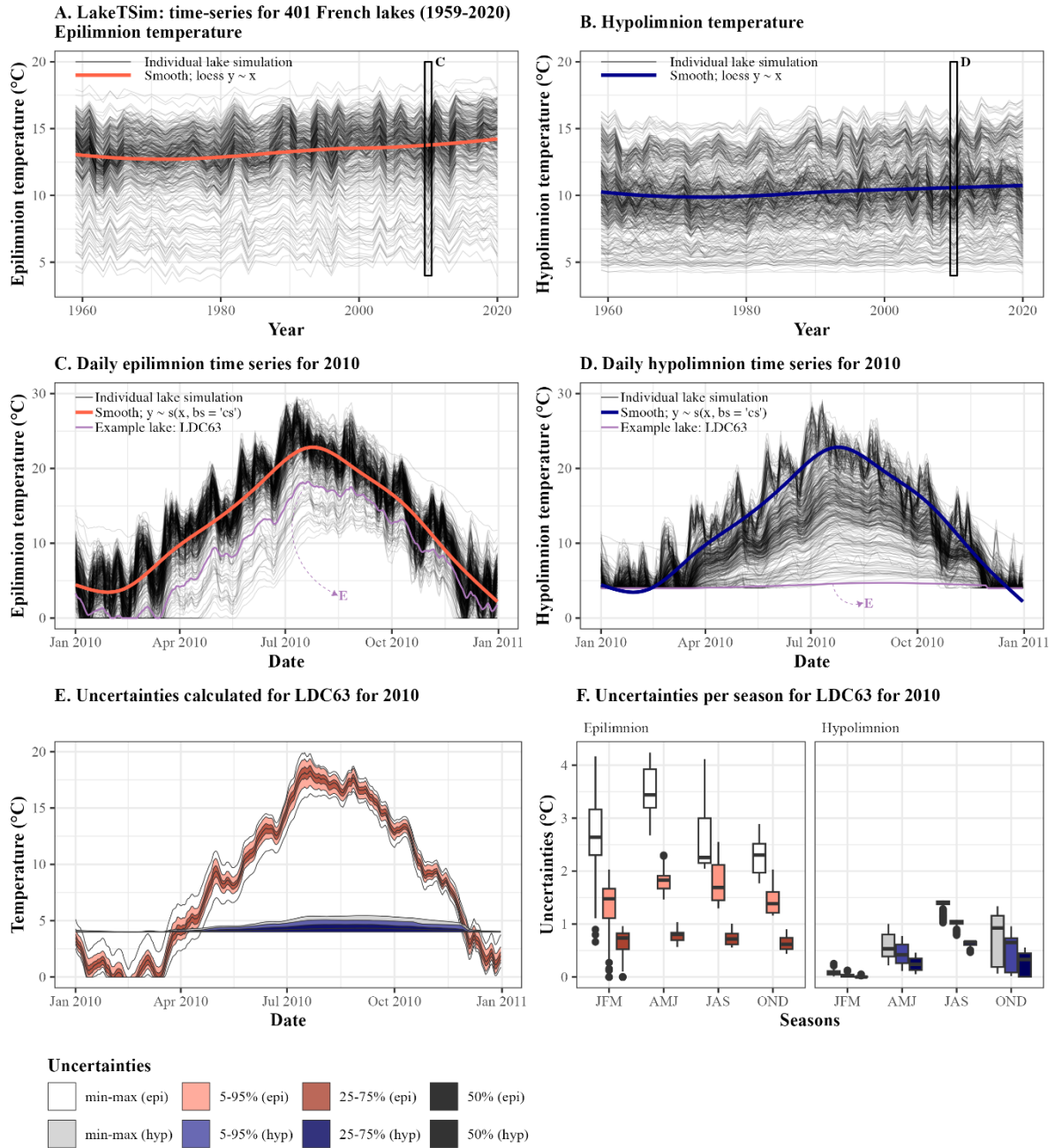


**Figure 2: Presentation of the LakeTSim data. (A) Epilimnion and (B) hypolimnion mean annual temperatures, with average trend across lakes shown with a smooth spline. (C) Daily epilimnion temperature per lake in the dataset for 2010, with smooth spline and the time series for one lake (LDC63) highlighted. (D) Daily hypolimnion temperature per lake in the dataset for 2010, with smooth spline and the time series for one lake (LDC63) highlighted. LDC63 is the code for Lake Chauvet, a natural lake (45.46 °N, 2.83 °E) located at 1167 m asl, with a surface area of 0.51 km<sup>2</sup>, a volume of 17.41 10<sup>6</sup> m<sup>3</sup>, and a maximum depth of 66.8 m. The simulation for LDC63 was conducted resorting to SAFRAN data and was run with the “calibrated” mode. (E) Uncertainties were calculated per lake and per day and are shown here daily for LDC63, in 2010, for both the epilimnion (epi) and the hypolimnion (hyp). (F) Uncertainties are shown here seasonally for LDC63, in 2010, for both the epilimnion (epi) and the hypolimnion (hyp). JFM corresponds to January-February-March, AMJ corresponds to April-May-June, JAS corresponds to July-August-September and OND corresponds to October-November-December.**

**Table 1: Characteristics of the lakes simulated with the OKPLM in “default” and “calibrated” modes with SAFRAN and S2M meteorological data for the period 1959-2020;  $n$  represents the number of lakes.**

Variables	Minimal - Maximal range			
Model parameters	Default		Calibrated	
Meteorological data	SAFRAN	S2M	SAFRAN	S2M
$n$	210	21	164	6
Altitude (m)	1 - 1753	916 - 2213	0 - 2279.7	1577.5 - 2172.5
Latitude (°N)	41.47 - 50.87	42.55 - 46.21	42.88 - 49.87	42.65 - 42.86
Longitude (°E)	-3.90 - 9.48	0.08 - 6.94	-4.24 - 6.96	-0.33 - 1.92
Maximal depth (m)	0.8 - 309.7	10.3 - 180	1.2 - 124	49 - 112
Surface area (km <sup>2</sup> )	0.08 - 577.12	0.11 - 6.52	0.29 - 57.57	0.45 - 1.21
Volume (m <sup>3</sup> )	$5 \times 10^4 - 8.9 \times 10^{10}$	$51.4 \times 10^4 - 33.32 \times 10^7$	$12.9 \times 10^4 - 49.88 \times 10^7$	$72.7 \times 10^5 - 68.6 \times 10^6$

268

### 269 3.5. Calibration, uncertainty and sensitivity analysis

270 Calibration, uncertainty and sensitivity analyses of model parameters were carried out using the package “CUSPY”  
 271 (Calibration, Uncertainty analysis and Sensitivity analysis in PYthon), which is part of the software suite  
 272 “ALAMODE” (Danis, 2020) and acts as an interface to the package “pyemu” (White et al., 2016, 2020). In addition  
 273 to model parameters, sensitivity analysis was extended to encompass forcing parameters (*MAAT*, *at\_factor*,  
 274 *sw\_factor*) as they provide information about the degree of sensitivity exhibited by model parameters in response  
 275 to biases in the forcing data.

276 Parameter values were calibrated for lakes with available in situ data (temperature profiles and bathymetry).  
 277 Parameter values were calibrated using the Gauss-Levenberg-Marquardt algorithm and Tikhonov regularization  
 278 (White et al., 2020), and the squared sum of residuals as objective function. In addition to the calibrated parameter  
 279 values, the calibration process also provided posterior parameter uncertainty and composite scaled sensitivities.  
 280 Composite scaled sensitivities (*CSS*) indicate the quantity of information provided by each parameter and the  
 281 sensitivity of the model to them (Ely, 2006). The parameters with higher *CSS* values will have a greater impact on  
 282 the resulting simulation compared to those with low *CSS* values. To determine the *CSS* values for each parameter,  
 283 the Dimensionless Scaled Sensitivities (*DSS*) are used. *DSS* indicate how important an observation or how sensitive  
 284 a simulated equivalent of an observation is in relation to the estimation of a parameter. Further information on  
 285 these statistical measures is available in Hill (1998) and Poeter & Hill (1997). The dimensionless scaled sensitivity  
 286 for  $i$  and  $j$ ,  $i$  being one of the observations and  $j$  being one of the parameters, is calculated as:

$$287 \quad DSS_{i,j} = \left[ \frac{\partial y'_i}{\partial b_j} \right] b_j w_i^{1/2} \quad (13)$$

288 where  $y'_i$  is the simulated value associated with the  $i$ th observation,  $b_j$  is the  $j$ th estimated parameter,  $\frac{\partial y'_i}{\partial b_j}$  is the  
289 sensitivity of the simulated value associated with the  $i$ th observation and  $w_i$  is the weight of the  $i$ th observation  
290 calculated based on the inverse of the variance-covariance matrix of the observation errors.

291 The *CSS* for parameter  $j$  is calculated from *DSS* as follows:

$$292 \quad CSS_j = \left[ \frac{\sum_{i=1}^{ND} (DSS_{ij})^2 |b|}{ND} \right]^{1/2} \quad (14)$$

293 where  $ND$  is the number of observations and  $\mathbf{b}$  is a vector of parameters values.

294 The uncertainty of the simulations (calibrated and default) was analyzed using Monte Carlo simulations. For each  
295 lake, 100 Monte Carlo simulations were carried by randomly selecting the value of the model parameters. Two  
296 parameters, *at\_factor* and *sw\_factor*, multiplying the meteorological input, were added to account for possible  
297 uncertainties in input data. For default simulations, the a priori distribution of the parameters was assumed to  
298 follow a normal distribution with the average value and lower and upper bounds shown in Table 2. The ranges for  
299 parameters  $A$ ,  $B$  and  $C$  were estimated as four times the standard deviation of the residuals of the formulas used to  
300 estimate them according to Prats & Danis (2019). The parameters  $D$ ,  $E$  and  $\beta$ , are expected to lie in the range 0-1  
301 for mathematical and physical reasons. However, their respective values are highly interdependent and are difficult  
302 to identify. Given their higher uncertainty, the full 0-1 range was explored. For *MAAT*, *at\_factor* and *sw\_factor*,  
303 reasonable ranges ( $\pm 10\%$ ) were chosen to account for meteorological data uncertainty (measurement error, errors  
304 in regionalization, etc.). For calibrated simulations, the distribution of the parameters was obtained from the  
305 calibration results.

306 In this study, the non-parametric Kendall's tau coefficient (significance level at 5%) was used to identify statistical  
307 associations between uncertainty values and *CSS* in respect to lake geomorphological characteristics (maximal  
308 depth, volume, surface area, latitude and altitude).

309

310

311

312

313

314

315

316

317

**Table 2: Characteristics of the a priori distributions of the model parameters. Parameters with a circumflex accent indicate parameter values estimated for a particular lake according to the regionalization formulas by Prats & Danis (2019).**

Parameter	Average value	Lower bound	Upper bound
<i>A</i>	$\hat{A}$	$\hat{A} - 2 \cdot 0.74$	$\hat{A} + 2 \cdot 0.74$
<i>B</i>	$\hat{B}$	$\hat{B} - 2 \cdot 0.08$	$\hat{B} + 2 \cdot 0.08$
<i>C</i>	$\hat{C}$	$\hat{C} - 2 \cdot 0.004$	$\hat{C} + 2 \cdot 0.004$
<i>D</i>	$\hat{D}$	0	1
<i>E</i>	$\hat{E}$	0	1
$\alpha$	$\hat{\alpha}$	0	$\hat{\alpha} + 2 \cdot 0.08$
$\beta$	$\hat{\beta}$	0	1
<i>MAAT</i>	$M\hat{AAT}$	$M\hat{AAT} - 2 \cdot 0.5$	$M\hat{AAT} + 2 \cdot 0.5$
<i>at_factor</i>	1	0.9	1.1
<i>sw_factor</i>	1	0.9	1.1

318

#### 319 4. Model performance

320 The performance of the OKPLM was assessed in Prats & Danis (2019) by comparing its performance to two other  
321 often-applied models in lake studies, air2water (the 4-parameter version) and FLake. The air2water model is a  
322 semi-empirical model used to calculate the epilimnion temperature of temperate lakes (Toffolon et al., 2014;  
323 Piccolroaz et al., 2013). FLake is a one-dimensional (1D) hydrodynamic lake model for simulating temperature  
324 vertical profiles and mixing conditions in lakes (Mironov, 2008). To assess their performances, the three models  
325 were run between 1999 and 2016 over two sets of French lakes of different types (reservoirs, natural lakes, ponds,  
326 quarry lakes and gravel pits): a group of five lakes with continuous profile measurements, and a group of 404 lakes  
327 with less frequent temperature measurements. The performance assessment was limited to the period of 1999-2016  
328 due to the availability of water temperature data (in situ and satellite) during that specific timeframe. The scarcity  
329 of in situ water temperature measurements before 1999 applies to the entire set of lakes. However, it is important  
330 to note that long-term in situ water temperature data is available for a few large lakes, which was used to assess  
331 the performance of the three models (Prats & Danis, 2015). The OKPLM was run with the “default” parameter  
332 values given by the parameterization in Prats & Danis (2019). The air2water parameter values were obtained as a  
333 function of lake depth from the parametrization presented in Toffolon et al. (2014), based on data from 14 lakes  
334 around the globe. In this case, the air2water model parameters were not calibrated due to the fact that the percentage  
335 of missing data within the LakeSST dataset employed in Prats & Danis (2019) exceeded 97% for most lakes.  
336 Beyond this threshold of 97% missing data, the performance of the calibrated 4-parameter version of the air2water  
337 model was found to be unsatisfactory (Piccolroaz, 2016). However, when evaluating the model performance with

338 the set of five lakes with continuous data, air2water was run using parameter values calibrated for the individual  
339 lakes available data. FLake does not have calibration parameters. Meteorological forcing (SAFRAN) consisted of  
340 air temperature for the air2water model; solar radiation, vapor pressure, cloud cover and wind speed for FLake;  
341 and air temperature and solar radiation for the OKPLM.

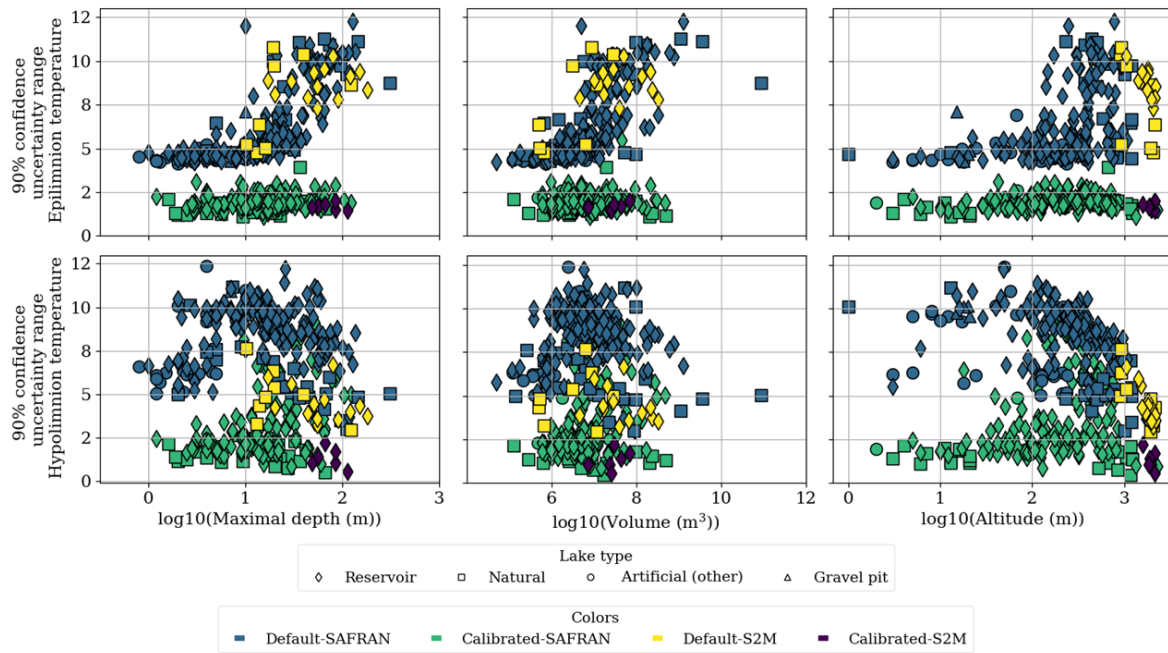
342 The OKPLM, air2water and FLake simulations were assessed through comparison to in situ measurements. For  
343 epilimnion temperatures, the average discrepancies calculated between OKPLM simulations and observations  
344 remained below 2 °C in most cases, in contrast to the air2water and FLake models. The performance comparison  
345 between the OKPLM, air2water and FLake yielded respectively median RMSE's (Root Mean Square Error) of  
346 1.7, 2.3 and 2.6 °C calculated between simulations and observations of epilimnion water temperature. Although  
347 when using calibrated parameter values for air2water, median RMSE was below 1 °C in most cases. For  
348 hypolimnion temperatures, the median RMSEs by lake type obtained with OKPLM simulations remained below  
349 2 °C, except for gravel pits (RMSE = 2.7 °C) and reservoirs (RMSE = 2.3 °C), whereas FLake yielded a median  
350 RMSE of 3.3 °C. For the epilimnion, the differences between the RMSE of lake types were not significant. In  
351 terms of depth, discrepancies between epilimnion temperature simulations with the OKPLM and measurements  
352 were highest for lakes with a depth > 10 m and for ponds around 1 m deep. The OKPLM simulations were also  
353 evaluated seasonally, in particular during summer and winter. The model simulated temperatures well with a  
354 median RMSE of 1.4 and 1.6 °C in summer and winter respectively.

## 355 5. Uncertainty analysis

356 Overall, for both simulations with default and calibrated model parameters, uncertainty was higher for  
357 hypolimnion temperature compared to epilimnion temperature especially in reservoirs (Figure 3). In default  
358 simulations, the uncertainty of simulated epilimnion temperatures showed a clear and strong relation with lake  
359 maximal depth (Figure 3, Table 3). On one hand, maximal depth had the highest Kendall's tau value of 0.64 ( $p$ -  
360 value < 0.0001), indicating a strong positive correlation with uncertainty followed by volume with a Kendall's tau  
361 of 0.59 ( $p$ -value < 0.0001). Uncertainty increased with maximal depth and volume in particular for lakes with  
362 depths greater than 10 m and volumes greater than  $10^6$  m<sup>3</sup> (Figure 3). Overall, lakes with higher maximal depths  
363 have higher volumes and are located at greater altitudes (Figures A1-A2 in Appendix A). On the other hand,  
364 moderate significant correlations were identified with surface area, altitude and latitude (Table 3). Lakes with  
365 larger surface areas and higher altitudes tend to have higher uncertainties whereas lakes located at higher latitudes  
366 tend to have lower uncertainties (Figure A3 in Appendix A). The latter can be linked to the fact that more shallow  
367 lakes are located at higher latitudes (Figure A1 in Appendix A). For default simulations of hypolimnion  
368 temperatures, uncertainty was maximal for lakes with depths around 10 m. Kendall's tau values revealed a  
369 moderate significant correlation between hypolimnion temperature uncertainty and altitude (-0.45,  $p$ -value <  
370 0.0001). The decrease in uncertainties with altitude can be related to the fact that lakes situated at very high  
371 altitudes are mostly deep. Further, in the present dataset, lakes with higher maximal depths occur as altitude  
372 increases (Figure A1-A2 in Appendix A).

373 After calibration, there was an important reduction in simulation uncertainty. For default simulations of epilimnion  
374 temperature the median of the 90% confidence uncertainty range was 5.42 °C, while after calibration it was 1.85  
375 °C. For hypolimnion temperature, the median of the 90% confidence uncertainty range of default simulations was  
376 8.5 °C, while it was 2.32 °C after calibration. However, many reservoirs with depths greater than 8 m still had a

377 much greater uncertainty (uncertainty range > 4 °C) than the rest of lakes after calibration. Additionally, reservoirs  
 378 (and a few natural lakes) above 100 m in altitude showed the highest uncertainties in the simulation of epilimnion  
 379 temperature.



380

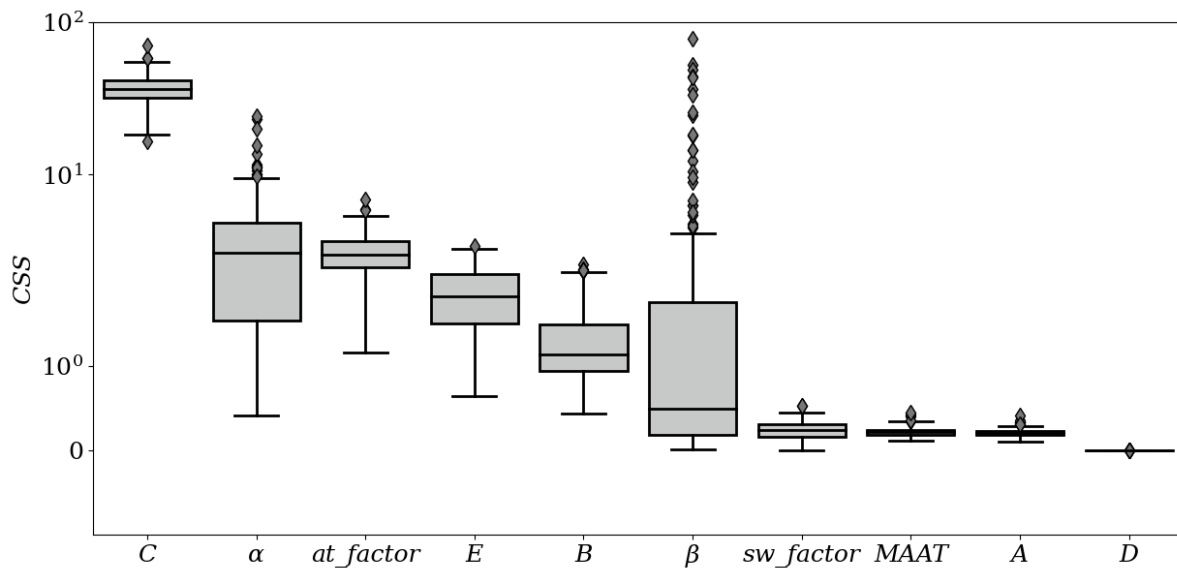
**Figure 3: Average 90% confidence uncertainty range for epilimnion (top panel) and hypolimnion (bottom panel) temperatures in calibrated ( $n = 170$ ) and default ( $n = 231$ ) simulations for the period 1959-2020. The “other” artificial lakes consist of ponds and quarry lakes.**

**Table 3: Kendall’s tau coefficients and  $p$ -values of average 90% confidence uncertainty range for epilimnion and hypolimnion temperatures obtained from default simulations (1959-2020) in respect to lakes geomorphological characteristics. For each lake, “Epilimnion uncertainty” and “Hypolimnion uncertainty” are defined as the average 90% confidence uncertainty range calculated as the difference between the 95<sup>th</sup> and 5<sup>th</sup> percentiles of the daily simulated epilimnion and hypolimnion water temperatures. The significance levels are represented as follows: \*:  $1.00e-02 < p\text{-value} \leq 5.00e-02$ , \*\*:  $1.00e-03 < p\text{-value} \leq 1.00e-02$ , \*\*\*:  $1.00e-04 < p\text{-value} \leq 1.00e-03$ , \*\*\*\*:  $p\text{-value} \leq 1.00e-04$ . Otherwise, correlations are not significant ( $p\text{-value} > 0.05$ ).**

	Maximal depth (m)	Surface area (km <sup>2</sup> )	Altitude (m)	Latitude (°N)	Volume (m <sup>3</sup> )
<b>Epilimnion uncertainty</b>	0.64****	0.31****	0.39****	-0.40****	0.59****
<b>Hypolimnion uncertainty</b>	-0.13**	0.05	-0.45****	0.03	-0.03

### 381 6. Sensitivity analysis

382 The parameter to which the model was most sensitive was the parameter  $C$  (Figure 4), which multiplies solar  
 383 radiation in Eq. (1). The  $CSS$  for  $C$  were an order of magnitude greater than for the next parameters with highest  
 384  $CSS$ , the parameter  $a$  and  $at\_factor$ , both influencing the effect of air temperature on simulated water temperature.  
 385 Other parameters to which the model was somewhat sensitive were  $E$ ,  $B$  and  $\beta$ . The model was quite insensitive  
 386 to  $sw\_factor$ ,  $MAAT$  and  $A$ . The parameter  $D$ , with  $CSS$  several orders of magnitude smaller than the other  
 387 parameters, was unidentifiable.



388

**Figure 4: Composite scaled sensitivities (CSS) for each parameter. The boxplots indicate the distribution of CSS between the simulations calibrated for different lakes. The y-axis is in logarithmic form.**

389 The model tended to be more sensitive to the parameter values in the case of reservoirs than in the case of natural  
 390 lakes (Figure 5, Figures A4-A7 in Appendix A). Some parameters showed a dependency on lakes  
 391 geomorphological characteristics. With the exception of a weak correlation with altitude (Kendall's tau = 0.18),  
 392 there was no significant dependence between the parameter C and lakes geomorphological characteristics (Table  
 393 4, Figure A4 in Appendix A). The parameter  $\alpha$  being parametrized as a function of lake volume, surface area and  
 394 altitude reflects the thermal inertia of the lake. It showed a clear highly significant dependency primarily on lake  
 395 depth (Kendall's tau = 0.47) followed by altitude (Kendall's tau = 0.4) and volume (Kendall's tau = 0.39) (Figure  
 396 5, Table 4). The increase of model sensitivity to the parameter  $\alpha$  primarily with depth as well as altitude and volume  
 397 propagated to the default simulations and explain the increased uncertainty with these same geomorphological  
 398 characteristics in the default simulations. The parameter *at\_factor*, was weakly but significantly correlated with  
 399 all lakes geomorphological characteristics except for latitude with which no correlation was found (Figure 5, Table  
 400 4, Figures A4-A7 in Appendix A). CSS were mostly low for the parameter  $\beta$ , except for a few reservoirs and  
 401 artificial lakes that scored very high CSS values. The sensitivity of  $\beta$  displayed a weak but significant correlation  
 402 with lakes geomorphological characteristics, except for volume (Table 4).

403 Although the model in general was not very sensitive to the values of the parameters most directly related with  
 404 hypolimnion temperatures (*D*, *E*,  $\beta$ ), the quality of hypolimnion temperature was greatly improved through  
 405 calibration. This would seem to indicate that the quality of simulated hypolimnion temperature was improved  
 406 through the improvement of epilimnion temperature simulations.

407

408

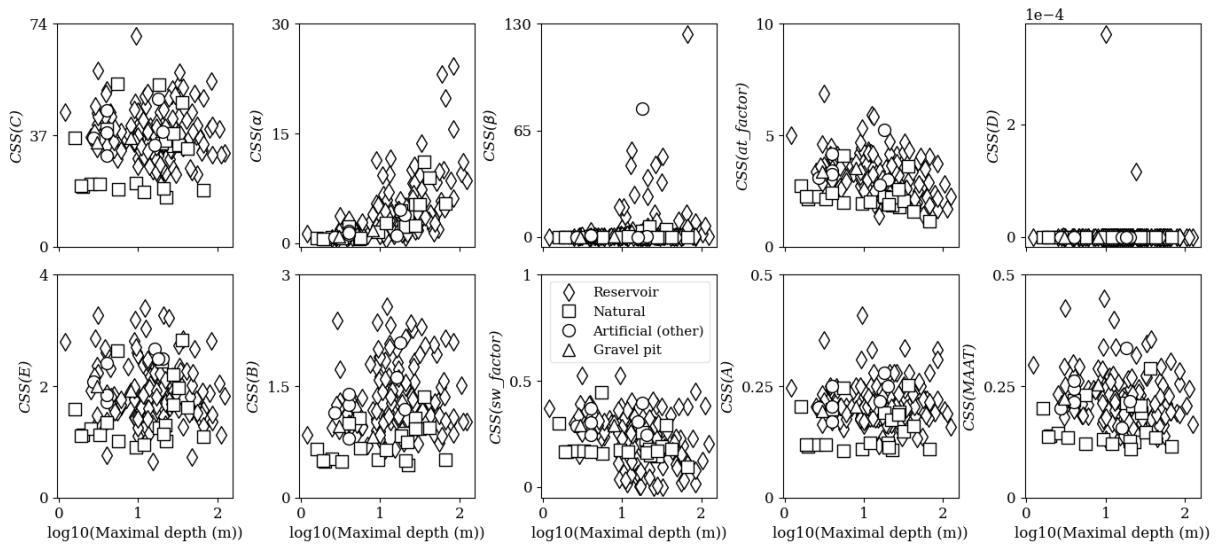
409

410

**Table 4: Kendall’s tau coefficients and  $p$ -values of  $CSS$  for model parameters values and drivers obtained from calibrated simulations (1959-2020) in respect to lakes geomorphological characteristics. The significance levels are represented as follows: \*:  $1.00e-02 < p\text{-value} \leq 5.00e-02$ , \*\*:  $1.00e-03 < p\text{-value} \leq 1.00e-02$ , \*\*\*:  $1.00e-04 < p\text{-value} \leq 1.00e-03$ , \*\*\*\*:  $p\text{-value} \leq 1.00e-04$ . Otherwise, correlations are not significant ( $p\text{-value} > 0.05$ ).**

	Maximal depth (m)	Surface area (km <sup>2</sup> )	Altitude (m)	Latitude (°N)	Volume (m <sup>3</sup> )
$CSS_A$	0.02	-0.1	0.14**	-0.08	-0.07
$CSS_B$	0.09	-0.04	0.14**	-0.14**	0.02
$CSS_C$	-0.04	-0.09	0.18***	-0.05	-0.1
$CSS_D$	-0.12*	0.02	-0.14**	0.06	-0.1
$CSS_E$	-0.01	-0.001	0.02	0.0003	-0.03
$CSS_\alpha$	0.47****	0.07	0.4****	-0.23****	0.39****
$CSS_\beta$	0.16**	-0.12*	0.22****	-0.19***	0.05
$CSS_{at\_factor}$	-0.25****	-0.14**	-0.13*	0.04	-0.28****
$CSS_{sw\_factor}$	-0.22****	-0.06	-0.14**	0.06	-0.2****
$CSS_{MAAT}$	-0.09	-0.13**	0.13*	-0.02	-0.15**

411



412

**Figure 5 : Composite scaled sensitivities ( $CSS$ ) for each model parameter as a function of maximal depth. The “other” artificial lakes consist of ponds and quarry lakes.**

## 413 7. Discussion and implications

414 Lakes are undeniably changing under climate change and long-term future projections show that the shifts in  
 415 ecosystem functioning will continue with aggravated alterations (Woolway & Merchant, 2019). In particular, given  
 416 the key role of lake water temperature in regulating ecosystem processes, its warming has become a response that  
 417 is crucial to monitor, explore and understand. Hence, the importance of developing or adopting approaches, such  
 418 as numerical models, that will provide long-term information about water temperature and allow us to understand  
 419 the thermal response of lakes to climate change.



420 Here we used a semi-empirical model, the OKPLM, to simulate six decades of epilimnion and hypolimnion water  
421 temperatures in French lakes. In comparison to similar models, overall, the OKPLM provides acceptable  
422 estimations of water temperatures, with better results for epilimnion temperatures. The values of the RMSEs  
423 provided in Prats & Danis (2019) and obtained between OKPLM simulations and observations are comparable to  
424 values found in studies applying complex hydrodynamic lake models (Read et al., 2014; Fang et al., 2012). When  
425 using the default parameter values, the uncertainty associated with epilimnion temperature simulations was  
426 significantly related to all geomorphological characteristics however, it was especially strongly correlated to lake  
427 maximal depth. In contrast, the uncertainty in the hypolimnion simulations had a significant correlation solely with  
428 altitude and maximal depth. The importance of this correlation was especially noteworthy in the case of reservoirs  
429 located in low-altitude regions where uncertainties were the lowest. While the association between hypolimnion  
430 uncertainty and maximal depth exhibited only a weak correlation, the instances of highest uncertainties were  
431 predominantly found in reservoirs having maximal depths around 10 m. The correlations found between lakes  
432 geomorphological characteristics and simulations uncertainties suggests that there might be systematic biases in  
433 the definition of model parameters or in the forcing data. The calibration of model parameters significantly reduced  
434 the uncertainties yet, for hypolimnion temperatures, they remained considerably high and increased with depth  
435 especially in reservoirs.

436 The high levels of uncertainty found in reservoirs could be somewhat attributed to the lack of consideration of  
437 water level fluctuations in the model. In contrast to other lakes (e.g., natural lakes, artificial lakes and gravel pits)  
438 reservoirs experience significant variations in their water level, which influences the heat budget and hence their  
439 thermal regime. Therefore, even under similar meteorological conditions lakes and reservoirs could have different  
440 thermal behaviors (Nowlin et al., 2004). In reservoirs, the discharge depth is a driver of thermal structure. Deep  
441 discharges could contribute to warmer bottom waters (Carr et al., 2020) whereas in some cases if the reservoir is  
442 shallow or if the discharge depth is not deep, it could demonstrate lake-like thermal behavior. This does not  
443 necessarily mean that, in this case, the entire functioning of the reservoir resembles one of a natural lake; there are  
444 still differences to consider (Detmer et al., 2022).

445 The application of the OKPLM should be made with caution given its performance and depending on the objective  
446 of the study. The model does not take into account a complete set of meteorological forcing (e.g., with cloud cover,  
447 relative humidity and wind speed and direction) or other variables (e.g., inflow and outflow rates or water level  
448 fluctuations, inflow discharge depth and inflow temperature) that could influence the thermal structure of the  
449 ecosystem (Yang et al., 2020; Carr et al., 2020). Furthermore, the OKPLM was parametrized for a specific set of  
450 lakes with particular geomorphological characteristics. Thus, it would be advisable to apply the model over lakes  
451 with similar characteristics. If the aim is to conduct a long-term regional or global study for studying general  
452 patterns of climate change impacts over a large number of study sites, the utilization of semi-empirical models  
453 such as the OKPLM is the most suitable choice. Although complex, deterministic or process-based models provide  
454 a more accurate representation of thermal conditions, applying these models over several study sites and for long  
455 periods is usually hindered by the scarcity of the required input data. The increased complexity of these models  
456 (with reference to an increased number of model parameters) is beneficial for representing additional ecosystem  
457 processes. Yet the greater number of model parameters, increases the sensitivity of models and demands more  
458 calibration efforts (Lindenschmidt, 2006). Furthermore, a reduction in model errors is sometimes associated with

459 an increased complexity in model structure; however, this is not always consistent since a complex model does  
460 not necessarily provide better estimations and thus lower errors than a simple model (Snowling and Kramer, 2001).

461 Our goal in publishing the present dataset is to expand knowledge about the water temperature of French lakes and  
462 provide data, with enough details and reliability, that it could be implemented in different studies where water  
463 temperature is implicated for understanding specific processes or interactions, in particular under climate change.  
464 Hence the significance of the present findings. The present study, making use of a semi-empirical model to provide  
465 long-term data about water temperature, was necessary for several reasons. Equipping a large number of lakes  
466 with thermal sensors is challenging and labor-intensive, it comes with a high financial cost that is often not  
467 available. Consequently, historical and even current water temperature datasets are often scarce, which can be  
468 problematic for studying the impact of climate change, as it requires high frequency data over a long duration of  
469 time for accurate analysis. In general, the higher the sampling frequency and duration, the better the data is suited  
470 to estimate or analyze specific processes or warming trends. The sampling frequency and length of a dataset have  
471 been shown to play a role in determining the accuracy of estimating warming trends where time series longer than  
472 30 years seem to be the most appropriate (Gray et al., 2018). Although, the duration and frequency of a dataset  
473 have a major role in reflecting accurate representations, their influence is scarcely addressed when it comes to  
474 climate change studies related to warming trends in water temperature.

475 This dataset will be useful for climate change studies; it could be used to develop and analyze several temperature  
476 indicators (e.g., annual or seasonal maximal and minimal temperature values, temperature exceeding certain  
477 thresholds with biological implications, etc.). Further, mixing and stratification dynamics are important to  
478 characterize as they drive lake biogeochemistry. Among other processes, they influence the distribution of  
479 nutrients, primary productivity and the composition of phytoplankton and zooplankton communities along the  
480 water column (Judd et al., 2005). With the LakeTSim dataset, it is possible to classify the mixing regime of lakes  
481 and investigate possible triggers of regime shifts.

## 482 **8. Data usage**

483 The LakeTSim dataset comprises water temperature simulations for natural lakes ( $n = 54$ ), reservoirs ( $n = 302$ ),  
484 gravel pits ( $n = 7$ ), and other artificial lakes (e.g., ponds and quarry lakes,  $n = 38$ ). The simulations are for both the  
485 epi- and hypolimnion. Lakes that are fully mixed throughout the year (typically, shallower lakes) have the same  
486 temperature value for both layers. More generally, the delta of temperature can be used to calculate mixing regimes  
487 (Sharaf et al., in prep.).

488 The lakes in the dataset were selected because they are monitored as part of the European Water Framework  
489 Directive (Directive 2000/60/EC). The majority of the 401 lakes are non-natural and some were only created after  
490 1959 (i.e., the start of our simulations). We compiled the initial temporal gap filling related to the initial filling  
491 years for 282 of these 347 non-natural lakes (269 reservoirs and 13 artificial lakes, Figure A8 in Appendix A) in  
492 Table S1 (see Supplement) to be used as a companion dataset to LakeTSim. The filling years were sourced from  
493 <https://www.barrages-cfbr.eu> for 179 of the lakes and from the PLAN\_DEAU database for 103 of the lakes; the  
494 information was not available for 33 reservoirs, 7 gravel pits and 25 other artificial lakes of the LakeTSim dataset.

495 The median filling date was 1962 and 67% of the lakes with known filling dates were filled by 1980. While the  
496 complete simulations ranging from 1959 to 2020 can also be used as theoretical lake temperature for comparison

497 across similar periods, we recommend that users of LakeTSim data for reservoir and artificial lake simulations  
498 consider the initial filling dates provided in Table S1 to filter out years from the simulations during which lakes  
499 were not filled yet.

500 Additionally, users should be aware that some reservoirs might be drained completely at certain intervals (e.g.,  
501 every 10 years) for maintenance and inspection purposes, and that this is not reflected in our dataset. Finally, as  
502 mentioned in the discussion, some of the lakes in the dataset experience artificial (e.g., in reservoirs) or natural  
503 (e.g., in some smaller ponds) water level fluctuations, and potential intermittent dry-periods lasting weeks or  
504 months; none of these hydrological processes are accounted for in the simulations.

## 505 **9. Code availability**

506 The respective codes for the “CUSPY” (Prats-Rodríguez and Danis, 2023a) and “OKPLM” (Prats-Rodríguez and  
507 Danis, 2023b) packages, which can be used to conduct sensitivity and uncertainty analysis and to run the OKP  
508 Lake Model, are available at <https://github.com/inrae/ALAMODE-cuspy> and  
509 <https://github.com/inrae/ALAMODE-okp> as well as ZENODO.

## 510 **10. Data availability**

511 The LakeTSim dataset (Sharaf et al., 2023) for epilimnion and hypolimnion water temperature simulations and  
512 supporting information are available at [doi:10.57745/OF9WXR](https://doi.org/10.57745/OF9WXR). The file “00\_Data\_description.txt” contains a  
513 description of the dataset. The geographical (longitude and latitude) and morphological (surface area, volume and  
514 maximal depth) data for the 401 lakes are presented in the file “01\_Lake\_data.txt” in addition to the name, type,  
515 altitude and the identification code for each lake. The data are located in two main folders: “02\_Temperature\_data”  
516 containing daily epilimnion (tepi) and hypolimnion (thyp) temperatures simulated with the OKPLM and  
517 “03\_Uncertainty\_data” containing daily tepi and thyp uncertainties. In each folder, the data for temperature  
518 simulations and their uncertainties are presented in text files available in the folders  
519 “00\_LakeTSim\_SAFRAN\_OKPdefault\_data”, “01\_LakeTSim\_SAFRAN\_OKPcalibrated\_data”,  
520 “02\_LakeTSim\_S2M\_OKPdefault\_data” and “03\_LakeTSim\_S2M\_OKPcalibrated\_data”. The name of each file  
521 within these folders includes the identification code of the lake. From 2024, the data will be visible from a  
522 dashboard. The link to the dashboard will be accessible from [data.ecla.inrae.fr](https://data.ecla.inrae.fr).

## 523 **11. Conclusions**

524 We present the LakeTSim dataset and the semi-empirical OKP Lake Model for simulating water temperature in  
525 lakes. We applied the model over a set of 401 French lakes for the period 1959-2020 to derive daily simulations  
526 of epilimnion and hypolimnion water temperatures, here referred to as the LakeTSim dataset. Previous efforts to  
527 assess the model’s performance show an overall acceptable representation of epilimnion and hypolimnion  
528 temperatures when compared to in situ measurements. The uncertainty analysis of simulations demonstrates that  
529 higher uncertainties are found for, by order of relative importance: (1) default simulations, (2) hypolimnion  
530 compared to epilimnion temperatures and, (3) deep lakes, in particular reservoirs (maximal depth greater than 10  
531 m for epilimnion temperature and around 10 m for hypolimnion temperature simulated with default model  
532 parameters). Although the calibration significantly decreases the uncertainties related to both the epilimnion and  
533 hypolimnion, in some cases they are still considerable in the hypolimnion. Based on these results and if enough  
534 observation data are available, optimally we recommend the use of the OKPLM for shallow (maximal depth < 8

535 m) lakes with calibrated model parameters. However, if applied in its default or even calibrated configuration over  
536 deep lakes, one should be aware of the presented limitations and address them in the analysis. The LakeTSim  
537 dataset is valuable for assessing the impact of climate change on lakes thermal functioning, which is often hindered  
538 by the lack of water temperature observations. The present dataset will provide new insights about the thermal  
539 behavior of French lakes, which can provide useful context for stakeholders as they design management strategies  
540 in a context of climate change.

541

542

543

544

545

546

547

548

549

550

551

552

553

554

555

556

557

558

559

560

561

562

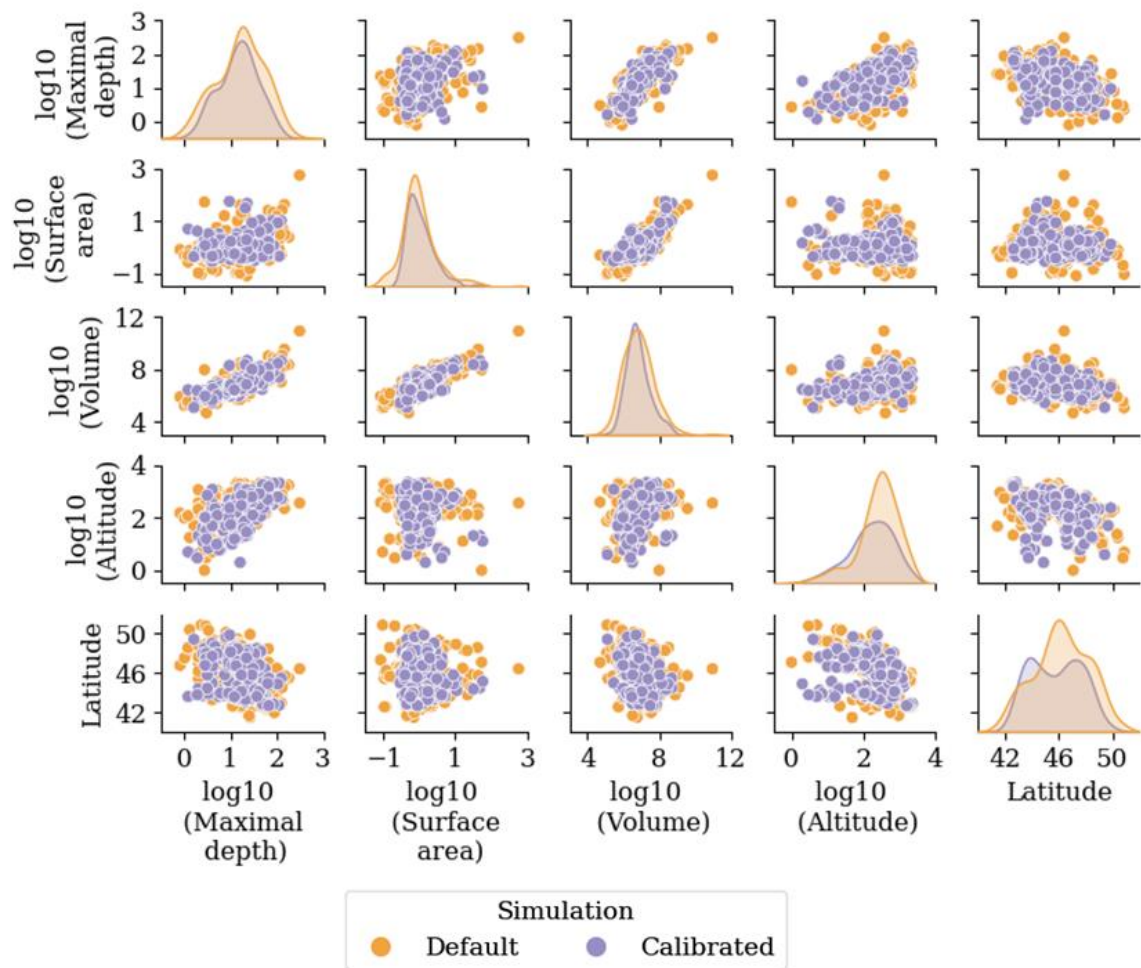
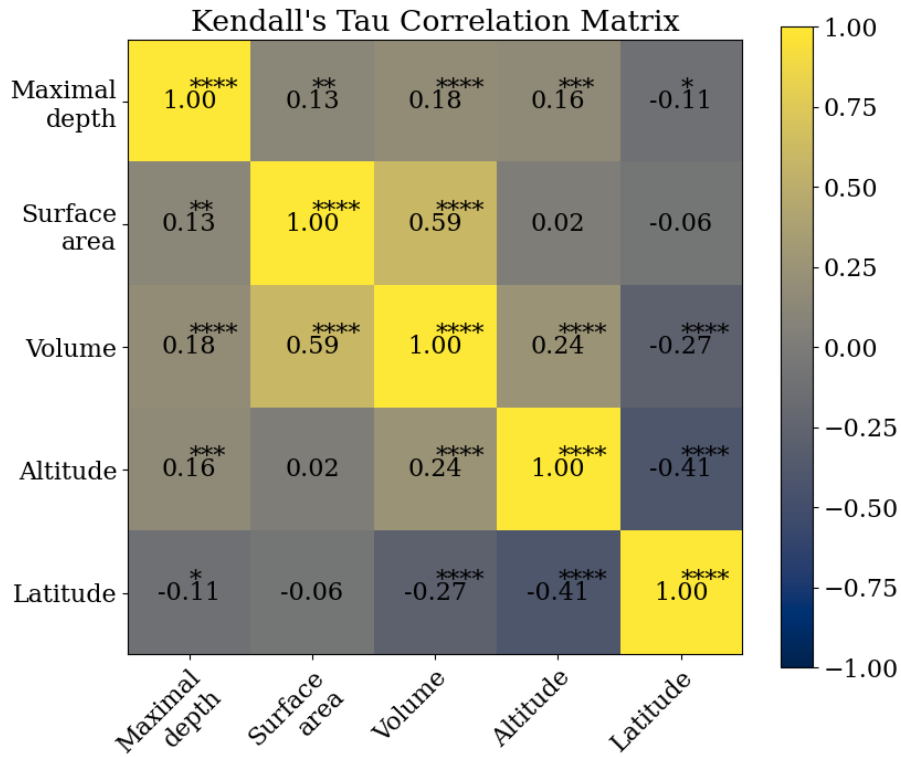
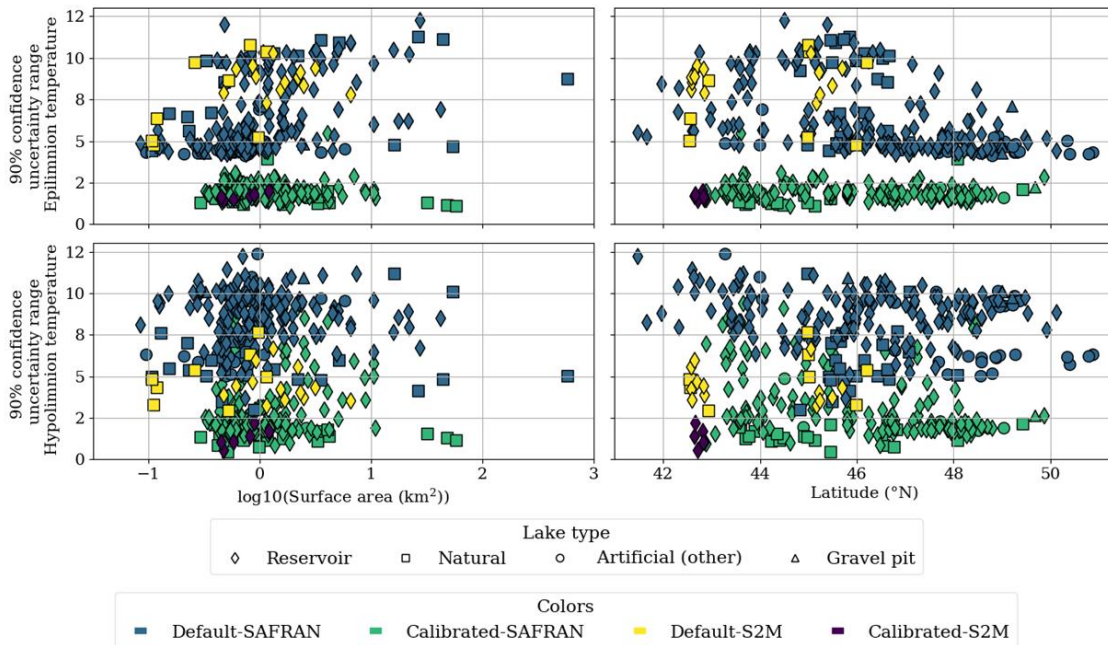


Figure A1: Scatter plots of lakes ( $n = 401$ ) geomorphological characteristics: Maximal depth (m), Surface area ( $\text{km}^2$ ), volume ( $\text{m}^3$ ), altitude (m) and latitude ( $^{\circ}\text{N}$ ).



**Figure A2:** Kendall’s tau correlation matrix of the geomorphological characteristics of lakes simulated in “default” mode ( $n = 231$ ): Maximal depth (m), Surface area (km<sup>2</sup>), volume (m<sup>3</sup>), altitude (m) and latitude (°N). The significance levels are represented as follows: \*:  $1.00e-02 < p\text{-value} \leq 5.00e-02$ , \*\*:  $1.00e-03 < p\text{-value} \leq 1.00e-02$ , \*\*\*:  $1.00e-04 < p\text{-value} \leq 1.00e-03$ , \*\*\*\*:  $p\text{-value} \leq 1.00e-04$ . Otherwise, correlations are not significant ( $p\text{-value} > 0.05$ ).



**Figure A3:** Average 90% confidence uncertainty range for epilimnion (top panel) and hypolimnion (bottom panel) temperatures in calibrated ( $n = 170$ ) and default ( $n = 231$ ) simulations for the period 1959-2020 as a function of surface area (km<sup>2</sup>) and latitude (°N). The “other” artificial lakes consist of ponds and quarry lakes.

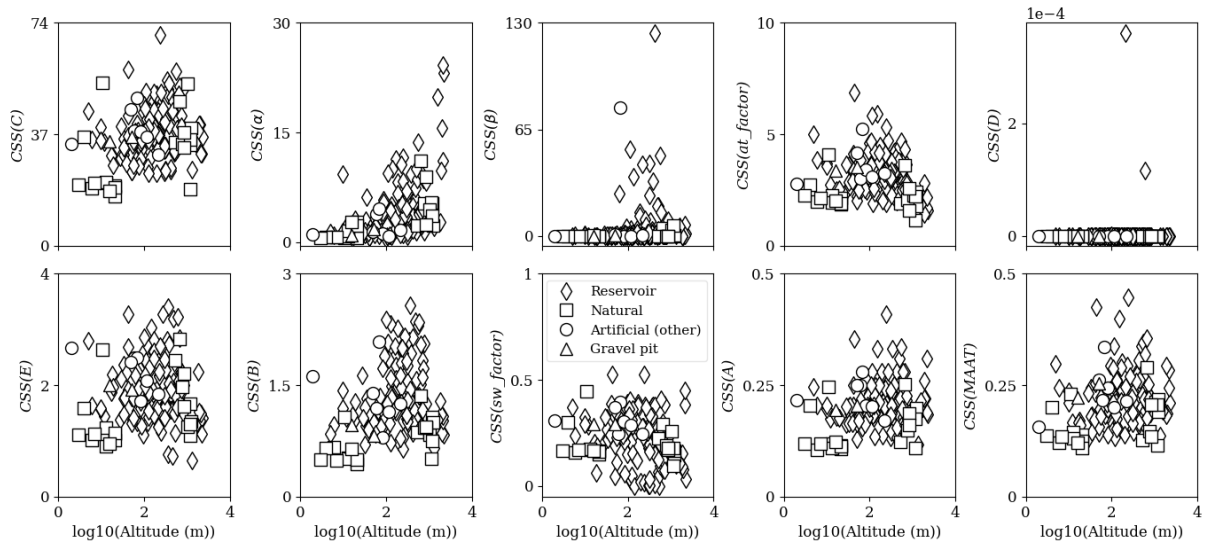


**Figure A4: Composite scaled sensitivities (CSS) for each model parameter as a function of altitude. The “other” artificial lakes consist of ponds and quarry lakes.**

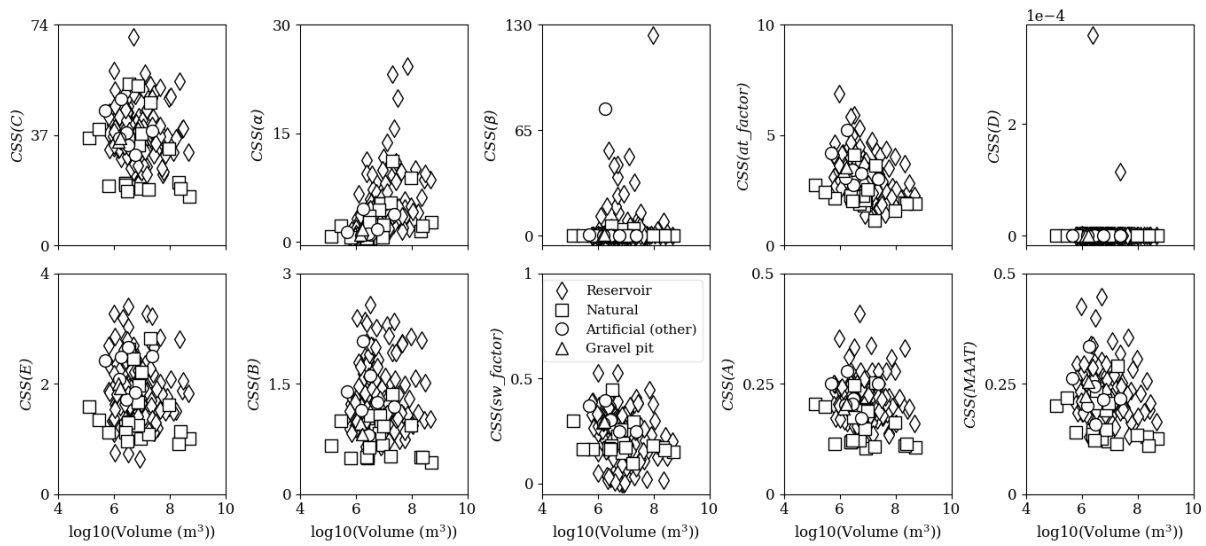


**Figure A5: Composite scaled sensitivities (CSS) for each model parameter as a function of volume. The “other” artificial lakes consist of ponds and quarry lakes.**

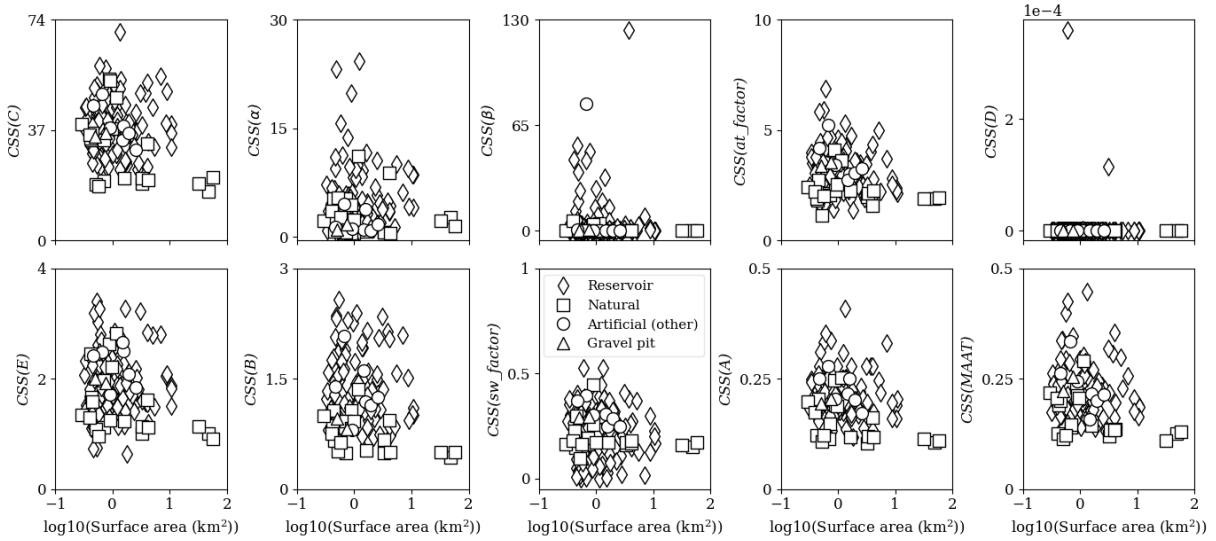


**Figure A6: Composite scaled sensitivities (CSS) for each model parameter as a function of surface area. The “other” artificial lakes consist of ponds and quarry lakes.**

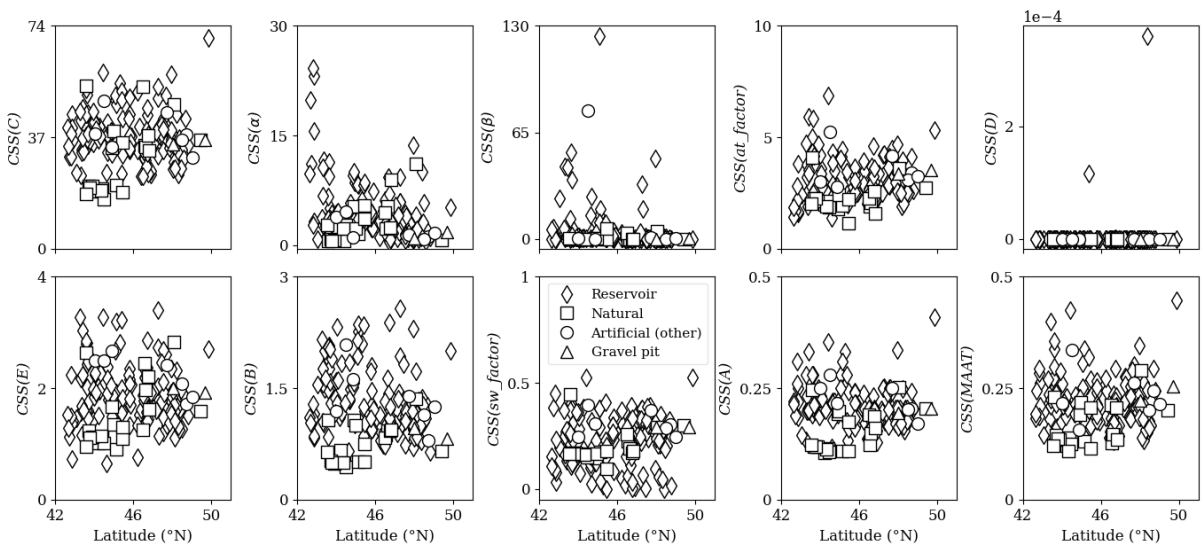
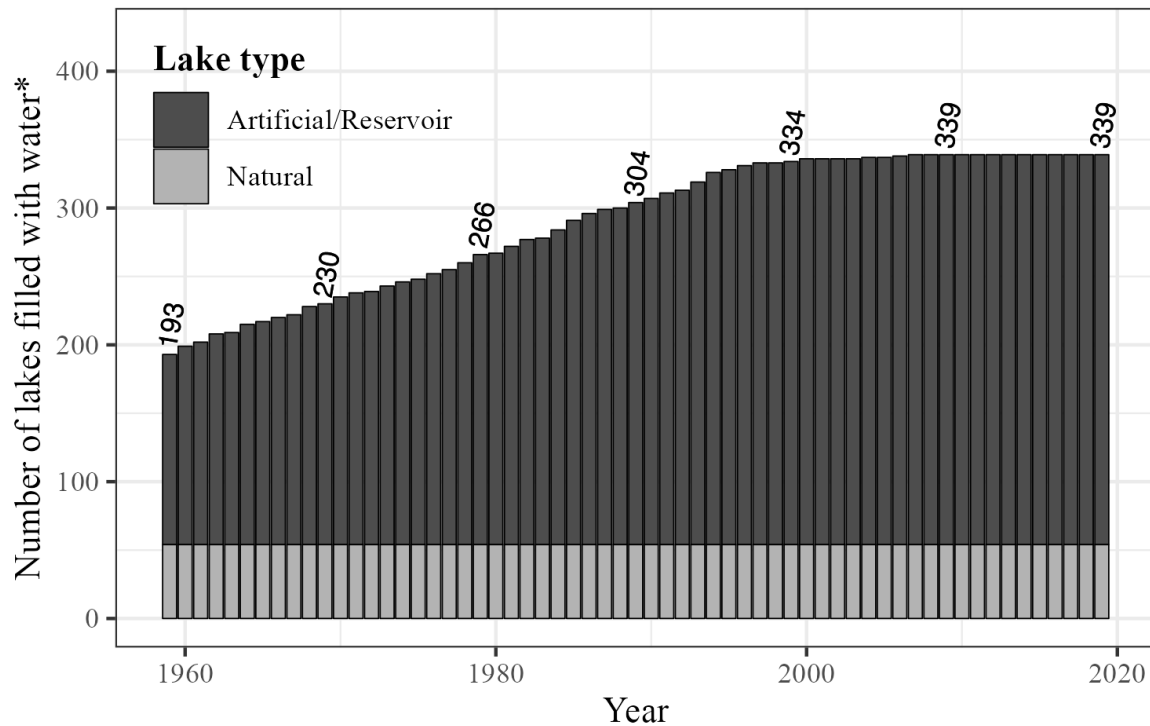


**Figure A7: Composite scaled sensitivities (CSS) for each model parameter as a function of latitude. The “other” artificial lakes consist of ponds and quarry lakes.**





\* 7 gravel pits, 33 reservoirs & 25 other artificial lakes with no information on filling year.

**Figure A8: Distribution of initial filling years for lakes (e.g., reservoirs, gravel pits, ponds and quarry lakes) of the LakeTSim dataset.**

### 565 13. Author contributions

566 NS wrote the original manuscript with input from JP and PAD. NS, JP and PAD discussed the results. JP developed  
 567 and carried out the implementation of the OKP Lake Model and the uncertainties computation in ALAMODE. JP  
 568 and NS performed the simulations and provided uncertainty analysis results with SAFRAN and S2M data  
 569 respectively. JP and NS implemented respectively the integration of SAFRAN and S2M data in ALAMODE. NS  
 570 prepared the LakeTSim dataset. JP and NS provided the uncertainty and sensitivity analysis. PAD designed,  
 571 contributed and supervised the implementation of S2M data in ALAMODE for forcing the OKPLM when  
 572 simulating high altitude lakes. PAD supervised the findings of this work. RB proposed and contributed to the  
 573 integration of the data consisting of initial filling dates of reservoirs and other artificial lakes in the manuscript.  
 574 NR and TT supervised and contributed to the implementation of simulation results in the database. NR processed  
 575 S2M data and compiled the data for initial filling years of reservoirs and other artificial lakes. NS, RB, and NR  
 576 prepared the figures. NR and TT prepared the doi for the LakeTSim dataset. TP conducted the fieldwork for the  
 577 monitoring, acquisition and verification of in situ temperature data. All authors reviewed, edited and approved the  
 578 final paper.

### 579 14. Competing interests

580 The authors declare that they have no conflict of interest.

581 **15. Acknowledgments**

582 The authors thank Météo-France for providing SAFRAN and S2M meteorological data, Matthieu Vernay for his  
583 feedback on the utilization of S2M data and the “Réseau Lacs Sentinelles” for providing bathymetry data for  
584 mountain lakes.

585 **16. Financial support**

586 The authors were supported by OFB (Office Français de la Biodiversité), SEGULA Technologies, INRAE (Institut  
587 National de Recherche pour l’Agriculture, l’Alimentation et l’environnement) and Pôle R&D ECLA  
588 (ECosystèmes LAcustres).

589 **17. References**

- 590 Adrian, R., O’Reilly, C. M., Zagarese, H., Baines, S. B., Hessen, D. O., Keller, W., Livingstone, D. M.,  
591 Sommaruga, R., Straile, D., Van Donk, E., Weyhenmeyer, G. A., and Winder, M.: Lakes as sentinels of climate  
592 change, *Limnol. Oceanogr.*, 54, 2283–2297, [https://doi.org/10.4319/lo.2009.54.6\\_part\\_2.2283](https://doi.org/10.4319/lo.2009.54.6_part_2.2283), 2009.
- 593 Allan, M. G., Hamilton, D. P., Trolle, D., Muraoka, K., and McBride, C.: Spatial heterogeneity in geothermally-  
594 influenced lakes derived from atmospherically corrected Landsat thermal imagery and three-dimensional  
595 hydrodynamic modelling, *Int. J. Appl. Earth Obs. Geoinf.*, 50, 106–116, <https://doi.org/10.1016/j.jag.2016.03.006>,  
596 2016.
- 597 Babbar-Sebens, M., Li, L., Song, K., and Xie, S.: On the Use of Landsat-5 TM Satellite for Assimilating Water  
598 Temperature Observations in 3D Hydrodynamic Model of Small Inland Reservoir in Midwestern US, *Adv.*  
599 *Remote Sens.*, 02, 214–227, <https://doi.org/10.4236/ars.2013.23024>, 2013.
- 600 Carr, M. K., Sadeghian, A., Lindenschmidt, K. E., Rinke, K., and Morales-Marin, L.: Impacts of Varying Dam  
601 Outflow Elevations on Water Temperature, Dissolved Oxygen, and Nutrient Distributions in a Large Prairie  
602 Reservoir, *Environ. Eng. Sci.*, 37, 78–97, <https://doi.org/10.1089/ees.2019.0146>, 2020.
- 603 Danis, P.: Rapport d ’avancement sur les outils de modélisation thermique, 1–8 pp., <https://doi.org/hal-03253847>,  
604 2020.
- 605 Daufresne, M., Lengfellner, K., and Sommer, U.: Global warming benefits the small in aquatic ecosystems, *Proc.*  
606 *Natl. Acad. Sci.*, 106, 12788–12793, <https://doi.org/10.1073/pnas.0902080106>, 2009.
- 607 Detmer, T. M., Parkos, J. J., and Wahl, D. H.: Long-term data show effects of atmospheric temperature anomaly  
608 and reservoir size on water temperature, thermal structure, and dissolved oxygen, *Aquat. Sci.*, 84, 1–13,  
609 <https://doi.org/10.1007/s00027-021-00835-2>, 2022.
- 610 Durand, Y., Brun, E., Merindol, L., Guyomarc’h, G., Lesaffre, B., and Martin, E.: A meteorological estimation of  
611 relevant parameters for snow models, *Ann. Glaciol.*, 18, 65–71, <https://doi.org/10.3189/S0260305500011277>,  
612 1993.
- 613 Ely, D. M.: Analysis of Sensitivity of Simulated Recharge to Selected Parameters for Seven Watersheds Modeled  
614 Using the Precipitation-Runoff Modeling System, U.S. Geological Survey Scientific Investigations Rep, 21 pp.,  
615 2006.
- 616 Fang, X., Alam, S. R., Stefan, H. G., Jiang, L., Jacobson, P. C., and Pereira, D. L.: Simulations of water quality  
617 and oxythermal cisco habitat in Minnesota lakes under past and future climate scenarios, *Water Qual. Res. J.*  
618 *Canada*, 47, 375–388, <https://doi.org/10.2166/wqrjc.2012.031>, 2012.
- 619 Gray, D. K., Hampton, S. E., O’Reilly, C. M., Sharma, S., and Cohen, R. S.: How do data collection and processing  
620 methods impact the accuracy of long-term trend estimation in lake surface-water temperatures?, *Limnol.*  
621 *Oceanogr. Methods*, 16, 504–515, <https://doi.org/10.1002/lom3.10262>, 2018.
- 622 Griffith, A. W. and Gobler, C. J.: Harmful algal blooms: A climate change co-stressor in marine and freshwater  
623 ecosystems, *Harmful Algae*, 91, 101590, <https://doi.org/10.1016/j.hal.2019.03.008>, 2020.
- 624 Halverson, G. H., Lee, C. M., Hestir, E. L., Hulley, G. C., Cawse-Nicholson, K., Hook, S. J., Bergamaschi, B. A.,  
625 Acuña, S., Tufillaro, N. B., Radocinski, R. G., Rivera, G., and Sommer, T. R.: Decline in Thermal Habitat  
626 Conditions for the Endangered Delta Smelt as Seen from Landsat Satellites (1985–2019), *Environ. Sci. Technol.*,

627 56, 185–193, <https://doi.org/10.1021/acs.est.1c02837>, 2022.

628 Havens, K. and Jeppesen, E.: Ecological responses of lakes to climate change, *Water*, 10, 917,  
629 <https://doi.org/10.3390/w10070917>, 2018.

630 Hill, M. C.: Methods and guidelines for effective model calibration: U.S. Geological Survey Water-Resources  
631 Investigations Report 98-4005, 90 pp., <https://doi.org/10.3133/wri984005>, 1998.

632 Hipsey, M. R., Bruce, L. C., Boon, C., Busch, B., Carey, C. C., Hamilton, D. P., Hanson, P. C., Read, J. S., De  
633 Sousa, E., Weber, M., and Winslow, L. A.: A General Lake Model (GLM 3.0) for linking with high-frequency  
634 sensor data from the Global Lake Ecological Observatory Network (GLEON), *Geosci. Model Dev.*, 12, 473–523,  
635 <https://doi.org/10.5194/gmd-12-473-2019>, 2019.

636 Janssen, A. B. G., Hilt, S., Kosten, S., de Klein, J. J. M., Paerl, H. W., and Van de Waal, D. B.: Shifting states,  
637 shifting services: Linking regime shifts to changes in ecosystem services of shallow lakes, *Freshw. Biol.*, 66, 1–  
638 12, <https://doi.org/10.1111/fwb.13582>, 2021.

639 Javaheri, A., Babbar-Sebens, M., and Miller, R. N.: From skin to bulk: An adjustment technique for assimilation  
640 of satellite-derived temperature observations in numerical models of small inland water bodies, *Adv. Water  
641 Resour.*, 92, 284–298, <https://doi.org/10.1016/j.advwatres.2016.03.012>, 2016.

642 Judd, K. E., Adams, H. E., Bosch, N. S., Kostrzewski, J. M., Scott, C. E., Schultz, B. M., Wang, D. H., and Kling,  
643 G. W.: A case history: Effects of mixing regime on nutrient dynamics and community structure in third sister lake,  
644 michigan during late winter and early spring 2003, *Lake Reserv. Manag.*, 21, 316–329,  
645 <https://doi.org/10.1080/07438140509354437>, 2005.

646 Kettle, H., Thompson, R., Anderson, N. J., and Livingstone, D. M.: Empirical modeling of summer lake surface  
647 temperatures in southwest Greenland, *Limnol. Oceanogr.*, 49, 271–282,  
648 <https://doi.org/10.4319/lo.2004.49.1.0271>, 2004.

649 Kharouba, H. M., Ehrlén, J., Gelman, A., Bolmgren, K., Allen, J. M., Travers, S. E., and Wolkovich, E. M.: Global  
650 shifts in the phenological synchrony of species interactions over recent decades, *Proc. Natl. Acad. Sci. U. S. A.*,  
651 115, 5211–5216, <https://doi.org/10.1073/pnas.1714511115>, 2018.

652 Kim, J., Seo, D., Jang, M., and Kim, J.: Augmentation of limited input data using an artificial neural network  
653 method to improve the accuracy of water quality modeling in a large lake, *J. Hydrol.*, 602, 126817,  
654 <https://doi.org/10.1016/j.jhydrol.2021.126817>, 2021.

655 Layden, A., Merchant, C., and Maccallum, S.: Global climatology of surface water temperatures of large lakes by  
656 remote sensing, *Int. J. Climatol.*, 35, 4464–4479, <https://doi.org/10.1002/joc.4299>, 2015.

657 Lind, L., Eckstein, R. L., and Relyea, R. A.: Direct and indirect effects of climate change on distribution and  
658 community composition of macrophytes in lentic systems, *Biol. Rev.*, 1686, 1677–1690,  
659 <https://doi.org/10.1111/brv.12858>, 2022.

660 Lindenschmidt, K. E.: The effect of complexity on parameter sensitivity and model uncertainty in river water  
661 quality modelling, *Ecol. Modell.*, 190, 72–86, <https://doi.org/10.1016/j.ecolmodel.2005.04.016>, 2006.

662 Mironov, D. V.: Parameterization of lakes in numerical weather prediction: Description of a lake model,  
663 *Encyclopedic Dictionary of Archaeology*, Offenbach, Germany: DWD, 2008.

664 Nouchi, V., Kutser, T., Wüest, A., Müller, B., Odermatt, D., Baracchini, T., and Bouffard, D.: Resolving  
665 biogeochemical processes in lakes using remote sensing, *Aquat. Sci.*, 81, 1–13, <https://doi.org/10.1007/s00027-019-0626-3>, 2019.

667 Nowlin, W. H., Davies, J. M., Nordin, R. N., and Mazumder, A.: Effects of water level fluctuation and short-term  
668 climate variation on thermal and stratification regimes of a British Columbia reservoir and lake, *Lake Reserv.  
669 Manag.*, 20, 91–109, <https://doi.org/10.1080/07438140409354354>, 2004.

670 Ottosson, F. and Abrahamsson, O.: Presentation and analysis of a model simulating epilimnetic and hypolimnetic  
671 temperatures in lakes, *Ecol. Modell.*, 110, 233–253, [https://doi.org/10.1016/S0304-3800\(98\)00067-2](https://doi.org/10.1016/S0304-3800(98)00067-2), 1998.

672 Piccolroaz, S.: Prediction of lake surface temperature using the air2water model: Guidelines, challenges, and future  
673 perspectives, *Adv. Oceanogr. Limnol.*, 7, 36–50, <https://doi.org/10.4081/aiol.2016.5791>, 2016.

674 Piccolroaz, S., Toffolon, M., and Majone, B.: A simple lumped model to convert air temperature into surface water

- 675 temperature in lakes, *Hydrol. Earth Syst. Sci.*, 17, 3323–3338, <https://doi.org/10.5194/hess-17-3323-2013>, 2013.
- 676 Piccolroaz, S., Woolway, R. I., and Merchant, C. J.: Global reconstruction of twentieth century lake surface water  
677 temperature reveals different warming trends depending on the climatic zone, *Clim. Change*, 160, 427–442,  
678 <https://doi.org/10.1007/s10584-020-02663-z>, 2020.
- 679 Pilla, R. M., Williamson, C. E., Adamovich, B. V., Adrian, R., Anneville, O., Chandra, S., Colom-Montero, W.,  
680 Devlin, S. P., Dix, M. A., Dokulil, M. T., Gaiser, E. E., Girdner, S. F., Hambright, K. D., Hamilton, D. P., Havens,  
681 K., Hessen, D. O., Higgins, S. N., Huttula, T. H., Huuskonen, H., Isles, P. D. F., Joehnk, K. D., Jones, I. D., Keller,  
682 W. B., Knoll, L. B., Korhonen, J., Kraemer, B. M., Leavitt, P. R., Lepori, F., Luger, M. S., Maberly, S. C., Melack,  
683 J. M., Melles, S. J., Müller-Navarra, D. C., Pierson, D. C., Pislegina, H. V., Plisnier, P.-D., Richardson, D. C.,  
684 Rimmer, A., Rogora, M., Rusak, J. A., Sadro, S., Salmaso, N., Saros, J. E., Saulnier-Talbot, É., Schindler, D. E.,  
685 Schmid, M., Shimaraeva, S. V., Silow, E. A., Sitoki, L. M., Sommaruga, R., Straile, D., Strock, K. E., Thiery, W.,  
686 Timofeyev, M. A., Verburg, P., Vinebrooke, R. D., Weyhenmeyer, G. A., and Zadereev, E.: Deeper waters are  
687 changing less consistently than surface waters in a global analysis of 102 lakes, *Sci. Rep.*, 10, 20514,  
688 <https://doi.org/10.1038/s41598-020-76873-x>, 2020.
- 689 Poeter, E. P. and Hill, M. C.: Inverse models: A necessary next step in ground-water modeling, *Groundwater*, 35,  
690 250–260, 1997.
- 691 Prats-Rodríguez, J. and Danis, P.-A.: inrae/ALAMODE-cuspy: cuspy v1.0,  
692 <https://doi.org/10.5281/ZENODO.7585606>, 2023a.
- 693 Prats-Rodríguez, J. and Danis, P.-A.: inrae/ALAMODE-okp: okplm v1.0,  
694 <https://doi.org/10.5281/ZENODO.7564750>, 2023b.
- 695 Prats, J. and Danis, P.-A.: Optimisation du réseau national de suivi pérenne in situ de la température des plans  
696 d'eau : apport de la modélisation et des données satellitaires, [Rapport Rech. irstea, 93, <https://doi.org/hal-02602604>, 2015.
- 698 Prats, J. and Danis, P. A.: An epilimnion and hypolimnion temperature model based on air temperature and lake  
699 characteristics, *Knowl. Manag. Aquat. Ecosyst.*, 8, <https://doi.org/10.1051/kmae/2019001>, 2019.
- 700 Prats, J., Reynaud, N., Rebière, D., Peroux, T., Tormos, T., and Danis, P. A.: LakeSST: Lake Skin Surface  
701 Temperature in French inland water bodies for 1999-2016 from Landsat archives, *Earth Syst. Sci. Data*, 10, 727–  
702 743, <https://doi.org/10.5194/essd-10-727-2018>, 2018.
- 703 Read, J. S., Winslow, L. A., Hansen, G. J. A., Van Den Hoek, J., Hanson, P. C., Bruce, L. C., and Markfort, C. D.:  
704 Simulating 2368 temperate lakes reveals weak coherence in stratification phenology, *Ecol. Modell.*, 291, 142–150,  
705 <https://doi.org/10.1016/j.ecolmodel.2014.07.029>, 2014.
- 706 Rimet, F., Anneville, O., Barbet, D., Chardon, C., Crépin, L., Domaizon, I., Dorioz, J. M., Espinat, L., Frossard,  
707 V., Guillard, J., Goulon, C., Hamelet, V., Hustache, J. C., Jacquet, S., Lainé, L., Montuelle, B., Perney, P., Quetin,  
708 P., Rasconi, S., Schellenberger, A., Tran-Khac, V., and Monet, G.: The Observatory on LAkes (OLA) database:  
709 Sixty years of environmental data accessible to the public, *J. Limnol.*, 79, 164–178,  
710 <https://doi.org/10.4081/jlimnol.2020.1944>, 2020.
- 711 Schaeffer, B. A., Iames, J., Dwyer, J., Urquhart, E., Salls, W., Rover, J., and Seegers, B.: An initial validation of  
712 Landsat 5 and 7 derived surface water temperature for U.S. lakes, reservoirs, and estuaries, *Int. J. Remote Sens.*,  
713 39, 7789–7805, <https://doi.org/10.1080/01431161.2018.1471545>, 2018.
- 714 Sharaf, N., Fadel, A., Bresciani, M., Giardino, C., Lemaire, B. J., Slim, K., Faour, G., and Vinçon-Leite, B.: Lake  
715 surface temperature retrieval from Landsat-8 and retrospective analysis in Karaoun Reservoir, Lebanon, *J. Appl.*  
716 *Remote Sens.*, 13, 1, <https://doi.org/10.1117/1.jrs.13.044505>, 2019.
- 717 Sharaf, N., Lemaire, B. J., Fadel, A., Slim, K., and Vinçon-Leite, B.: Assessing the thermal regime of poorly  
718 monitored reservoirs with a combined satellite and three-dimensional modeling approach, *Inl. Waters*, 11, 302–  
719 314, <https://doi.org/10.1080/20442041.2021.1913937>, 2021.
- 720 Sharaf, N., Prats, J., Reynaud, N., Tormos, T., Bruel, R., Peroux, T., and Danis, P. A.: LakeTSim (Lake  
721 Temperature Simulations), *Rech. Data Gouv*, <https://doi.org/doi:10.57745/OF9WXR>, 2023.
- 722 Sharma, S., Walker, S. C., and Jackson, D. A.: Empirical modelling of lake water-temperature relationships: A  
723 comparison of approaches, *Freshw. Biol.*, 53, 897–911, <https://doi.org/10.1111/j.1365-2427.2008.01943.x>, 2008.

724 Sharma, S., Gray, D. K., Read, J. S., O'Reilly, C. M., Schneider, P., Qudrat, A., Gries, C., Stefanoff, S., Hampton,  
725 S. E., Hook, S., Lenters, J. D., Livingstone, D. M., McIntyre, P. B., Adrian, R., Allan, M. G., Anneville, O., Arvola,  
726 L., Austin, J., Bailey, J., Baron, J. S., Brookes, J., Chen, Y., Daly, R., Dokulil, M., Dong, B., Ewing, K., De Eyto,  
727 E., Hamilton, D., Havens, K., Haydon, S., Hetzenauer, H., Heneberry, J., Hetherington, A. L., Higgins, S. N.,  
728 Hixson, E., Izmet'eva, L. R., Jones, B. M., Kangur, K., Kasprzak, P., Köster, O., Kraemer, B. M., Kumagai, M.,  
729 Kuusisto, E., Leshkevich, G., May, L., MacIntyre, S., Müller-Navarra, D., Naumenko, M., Noges, P., Noges, T.,  
730 Niederhauser, P., North, R. P., Paterson, A. M., Plisnier, P. D., Rigosi, A., Rimmer, A., Rogora, M., Rudstam, L.,  
731 Rusak, J. A., Salmaso, N., Samal, N. R., Schindler, D. E., Schladow, G., Schmidt, S. R., Schultz, T., Silow, E. A.,  
732 Straile, D., Teubner, K., Verburg, P., Voutilainen, A., Watkinson, A., Weyhenmeyer, G. A., Williamson, C. E.,  
733 and Woo, K. H.: A global database of lake surface temperatures collected by in situ and satellite methods from  
734 1985-2009, *Sci. Data*, 2, 1–19, <https://doi.org/10.1038/sdata.2015.8>, 2015.

735 Shatwell, T., Thiery, W., and Kirillin, G.: Future projections of temperature and mixing regime of European  
736 temperate lakes, *Hydrol. Earth Syst. Sci.*, 23, 1533–1551, <https://doi.org/10.5194/hess-23-1533-2019>, 2019.

737 Snowling, S. D. and Kramer, J. R.: Evaluating modelling uncertainty for model selection, *Ecol. Modell.*, 138, 17–  
738 30, [https://doi.org/10.1016/S0304-3800\(00\)00390-2](https://doi.org/10.1016/S0304-3800(00)00390-2), 2001.

739 Toffolon, M., Piccolroaz, S., Majone, B., Soja, A. M., Peeters, F., Schmid, M., and Wüest, A.: Prediction of surface  
740 temperature in lakes with different morphology using air temperature, *Limnol. Oceanogr.*, 59, 2185–2202,  
741 <https://doi.org/10.4319/lo.2014.59.6.2185>, 2014.

742 Vernay, M., Lafaysse, M., Mérindol, L., Giraud, G., and Morin, S.: Ensemble forecasting of snowpack conditions  
743 and avalanche hazard, *Cold Reg. Sci. Technol.*, 120, 251–262, <https://doi.org/10.1016/j.coldregions.2015.04.010>,  
744 2015.

745 Vernay, M., Lafaysse, M., Monteiro, D., Hagenmuller, P., Nheili, R., Samacoïts, R., Verfaillie, D., and Morin, S.:  
746 The S2M meteorological and snow cover reanalysis over the French mountainous areas: description and evaluation  
747 (1958-2021), *Earth Syst. Sci. Data*, 14, 1707–1733, <https://doi.org/10.5194/essd-14-1707-2022>, 2022.

748 White, J. T., Fienen, M. N., and Doherty, J. E.: A python framework for environmental model uncertainty analysis,  
749 *Environ. Model. Softw.*, 85, 217–228, <https://doi.org/10.1016/j.envsoft.2016.08.017>, 2016.

750 White, J. T., Hunt, R. J., Fienen, M. N., Doherty, J. E., and Survey, U. S. G.: Approaches to highly parameterized  
751 inversion: PEST++ Version 5, a software suite for parameter estimation, uncertainty analysis, management  
752 optimization and sensitivity analysis., *U.S. Geological Survey Techniques and Methods 7C26*, 52 pp.,  
753 <https://doi.org/10.3133/tm7C26>, 2020.

754 Woolway, R. I. and Merchant, C. J.: Worldwide alteration of lake mixing regimes in response to climate change,  
755 *Nat. Geosci.*, 12, 271–276, <https://doi.org/10.1038/s41561-019-0322-x>, 2019.

756 Woolway, R. I., Sharma, S., and Smol, J. P.: Lakes in Hot Water : The Impacts of a Changing Climate on Aquatic  
757 Ecosystems, *Bioscience*, <https://doi.org/10.1093/biosci/biac052>, 2022.

758 Yang, K., Yu, Z., Luo, Y., Yang, Y., Zhao, L., and Zhou, X.: Spatial and temporal variations in the relationship  
759 between lake water surface temperatures and water quality - A case study of Dianchi Lake, *Sci. Total Environ.*,  
760 624, 859–871, <https://doi.org/10.1016/j.scitotenv.2017.12.119>, 2018.

761 Yang, K., Yu, Z., and Luo, Y.: Analysis on driving factors of lake surface water temperature for major lakes in  
762 Yunnan-Guizhou Plateau, *Water Res.*, 184, 116018, <https://doi.org/10.1016/j.watres.2020.116018>, 2020.

763